catalysts

MDPI

Review

Recent Advances in Graphene Based TiO_2 Nanocomposites ($GTiO_2Ns$) for Photocatalytic Degradation of Synthetic Dyes

Rita Giovannetti *, Elena Rommozzi, Marco Zannotti and Chiara Anna D'Amato

School of Science and Technology, Chemistry Division, University of Camerino, Via S. Agostino 1, 62032 Camerino, Italy; elena.rommozzi@unicam.it (E.R.); marco.zannotti@unicam.it (M.Z.); chiaraanna.damato@unicam.it (C.A.D.)

* Correspondence: rita.giovannetti@unicam.it; Tel.: +39-0737-402272

Academic Editors: Ewa Kowalska, Marcin Janczarek and Agata Markowska-Szczupak
Received: 24 August 2017; Accepted: 10 October 2017; Published: 16 October 2017

Abstract: Synthetic dyes are widely used in textile, paper, food, cosmetic, and pharmaceutical industries. During industrial processes, some of these dyes are released into the wastewater and their successive release into rivers and lakes produces serious environmental problems. TiO_2 is one of the most widely studied and used photocatalysts for environmental remediation. However, it is mainly active under UV-light irradiation due to its band gap of 3.2 eV, while it shows low efficiency under the visible light spectrum. Regarding the exploration of TiO_2 activation in the visible light region of the total solar spectrum, the incorporation of carbon nanomaterials, such as graphene, in order to form carbon-TiO_2 composites is a promising area. Graphene, in fact, has a large surface area which makes it a good adsorbent for organic pollutants removal through the combination of electrostatic attraction and π-π interaction. Furthermore, it has a high electron mobility and therefore it reduces the electron-hole pair recombination, improving the photocatalytic activity of the semiconductor. In recent years, there was an increasing interest in the preparation of graphene-based TiO_2 photocatalysts. The present short review describes the recent advances in TiO_2 photocatalyst coupling with graphene materials with the aim of extending the light absorption of TiO_2 from UV wavelengths into the visible region, focusing on recent progress in the design and applications in the photocatalytic degradation of synthetic dyes.

Keywords: titanium dioxide; graphene; photocatalysis; visible light; dyes

1. Introduction

One of the biggest problems that the world is facing today is environmental pollution, which increases every year and causes serious and irreparable damage to the Earth [1]. Therefore, environmental protection and a new approach in environmental remediation are important factors for a real improvement in quality of life and for sustainable development.

In recent years, a large number of research activities have been dedicated to environmental protection and remediation as a consequence of special attention from social, political, and legislative authorities, which has led to the delivery of very stringent regulations for the environment [2].

Due to industrialization and the lack of effective treatments of the effluents at the source, a severe deterioration of freshwater resources caused by the release of a wide range of hazardous substances into water bodies has occurred. Of these substances, synthetic dyes represent a large group and therefore deserve particular attention, due to the high quantity—more than 800,000 tons—that is produced annually worldwide [3]. About one third of these is released into receiving waters every year through industrial wastewater discharges [4], which may have a severe influence on both the environment

and human health, affecting photosynthetic activity as well as dissolved oxygen concentration, and therefore causing serious ecologic problems [5].

Dyes present high toxicity, are carcinogenic and mutagenic in nature, and can also result in bioaccumulation in the food chain [6]. Because their origin is synthetic, these compounds are very stable in the presence of light and biodegradation [7]. Furthermore, very low concentrations of these are easily visible in contaminated waters; therefore, the total effect of the presence of dyes in the water ecosystem is both environmentally and aesthetically unacceptable.

Taking account of these considerations, there is an urgent need to develop new methods for the treatment of industrial wastewater containing synthetic dyes.

In recent years, photocatalysis studies have focused on the use of semiconductor materials as photocatalysts for environmental remediation. Semiconductor photocatalysis is a versatile, low-cost, and environmentally friendly treatment technology for many pollutants [8,9], and the use of heterogeneous photocatalysis is an emerging application in water decontamination.

Within a great number of oxide semiconductors, TiO_2 is the most widely used as promising photocatalyst, demonstrating a very important role in environmental remediation [10,11], solar energy [12], and other fields [13,14] due to its nontoxicity, low cost, corrosion resistance, abundant resources, and high photocatalytic efficiency [15–17].

A high number of studies concerning TiO_2 regard wastewater treatments [18–21] and, in many cases, total mineralization of pollutants without any waste disposal problem have been published [22]. On the other hand, the practical applications of this technique are limited to a narrow excitation wavelength because of a large band gap energy (3.2 eV), high recombination rate of the photo-produced electron–hole pair, and poor adsorption capacity [23–25]. In recent decades, various attempts have been applied to improve the catalytic efficiency of TiO_2 [18,26,27].

Due to its wide band-gap, TiO_2 is active only under UV-light irradiation; considering that the percentage of UV-light is less than 5% of the total incident solar spectrum on the Earth, in recent years research has focused on extending the light absorption of TiO_2 under visible light. The research goal of TiO_2 photocatalysis, as for other semiconductors, is represented by the combination of TiO_2 with other nanomaterials to achieve both visible light activation and adsorption capacity improvement, with the simultaneous limitation of the electron-hole recombination rate. For this reason, to improve the photocatalytic performances in the use of TiO_2, different approaches have been investigated, such as the use of co-catalysts, and loading with noble metal particles, dye, metallic or non-metallic doping [28–36]. Recently, enhancements of the photocatalytic activity of TiO_2 by visible light have been also demonstrated by the modification of TiO_2 with carbonaceous substances such as fullerenes, carbon nanotubes, and graphene to form carbon-TiO_2 composites [37–40].

In particular, graphene nanomaterials in combination with TiO_2 highlight new prospectives in the field of photocatalysis for their large specific surface area, flexible structure, extraordinary mobility of charge carriers at room temperature, high thermal and electrical conductivities, and high chemical stability [41–48], emerging as one of the most promising materials for enhancing the photocatalytic performance in the new generation of photocatalysts [49–56].

In this short review, the recent research advances in graphene-TiO_2 employed in photocatalysis are presented with the aim of extending the light absorption of TiO_2 from UV wavelengths into the visible region, as well as increasing the photocatalytic activity of the compound, focusing on the applications of synthetic dye degradation.

2. Graphene Materials: Concepts and Properties

Graphene (G) is the term used to indicate carbon atoms tightly packed in a plane monolayer into a two-dimensional (2D) "honeycomb lattice" that represents the building block for all graphitic materials such as fullerenes, nanotubes, and graphite [48,57].

The isolation of graphene from graphite in 2003, by Prof. Andre Geim and Prof. Kostya Novoselov, which was the first paper published in Science in 2004 [42] and was awarded the Nobel Prize in Physics

in 2010, has fascinated and revolutionized the scientific community [42,58,59]. This is due to graphene's notable properties and to the high range of applications that these properties offer to technologies such as energy storage and photocatalysis [60–67].

The IUPAC commission proposed the term "graphene" to substitute the older term "graphite layers", which was inappropriate in the research of two-dimensional (2D) monolayers of carbon atoms because the three-dimensional (3D) stacking structure is identified as "graphite" [59].

After the first report on graphene, which was obtained manually by mechanical cleavage with a Scotch tape sample of graphite, various techniques developed to produce thin graphitic films have been reported [55,68,69]. These can be divided into two main groups: bottom-up and top-down methods [55,69], as schematized in Figure 1.

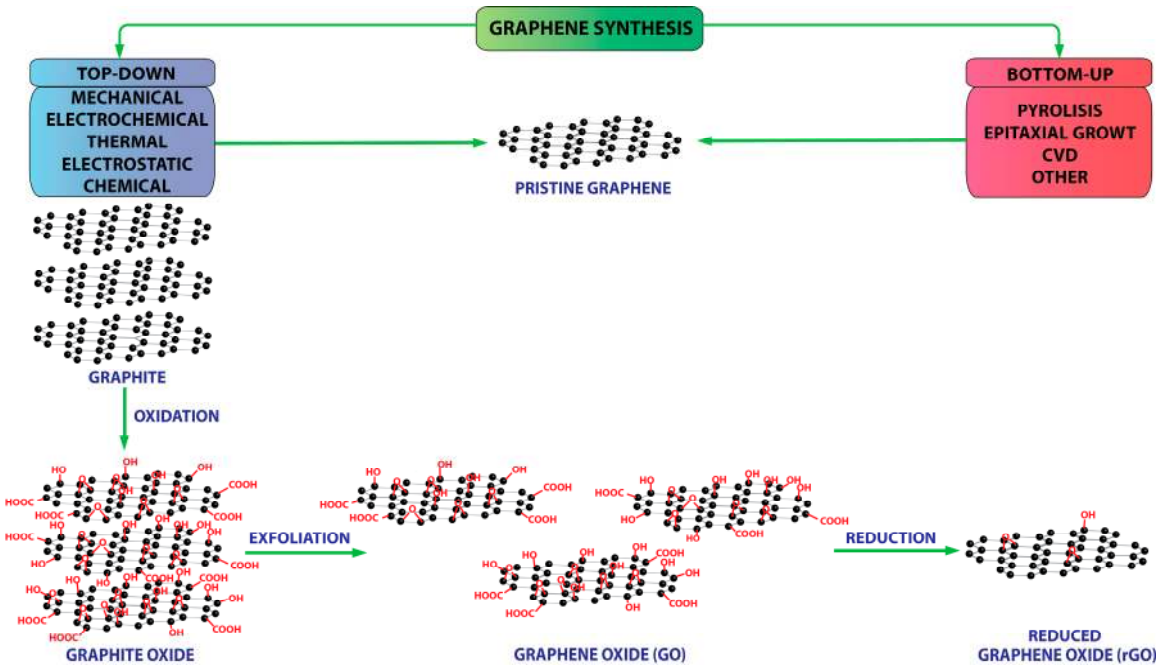

Figure 1. Schematic graphene synthesis: top-down and bottom-up methods.

In the bottom-up growth of graphene sheets (Table 1), the synthesis of graphene [70] can be obtained via epitaxial growth [71–73], chemical vapor deposition (CVD) [74–82], electrochemical reduction of CO and CO_2 [83,84], arc discharge [85,86], unzipping carbon nanotubes [70,87], organic synthesis [88], and pyrolysis [89–91].

The top-down approach (Table 2) offers considerable economic advantages over bottom-up methods [92,93], producing high quality graphene. In this case, the graphene is derived from the exfoliation of graphite, from mechanical [42,94–97], electrochemical expansion [98–100], thermal [101], electrostatic deposition [102], and chemical synthesis [103–105]. Some other techniques are unzipping nanotube [106–108] and microwave synthesis [109,110], or by chemical and/or thermal graphene oxide (GO) reduction [111]. This last method allows the production of low-cost and large-scale graphene, though with oxygen-containing groups and defects [112,113]. Much interest is directed at the study of proceedings to obtain graphene in the form of highly reduced graphene oxide (rGO) [114,115] or chemically modified graphene [116,117] from the oxidation and exfoliation of graphite and successive chemical reduction.

Table 1. Graphene synthesis with the bottom-up approach.

		Results	Highlight	Refs.
Epitaxial growth	-	General	Experimental and theoretical aspect	[71]
	-	Flower defects and effects of G grown on SiC substrate	Enhancements in the electronic properties of G-based devices	[72]
	-	G nanoribbons (GNR) on surface facets of SiC(0001)	Influence of the substrate step height on the energy barrier	[73]
Chemical vapor deposition (CVD)	-	Large-size, single-crystal, twisted bilayer G	Raman spectra measured as a function of the rotation angle	[74]
	-	G	Review: challenges and future perspective	[75]
	-	G on Ni and Cu substrates	Representative applications	[76]
	-	200 mm G on Ge(001)/Si(001) wafers	Absence of metallic contaminations	[77]
	-	Multilayer G films	Educational experiments: economical, safe, and simple technique in 30–45 min	[78]
	-	Large-scale G films on thin Ni layers	Two methods to shape and transfer films to specific substrates	[79]
	-	Monolayer G films on SiC(0001)	Ex-situ graphitization in argon atmosphere	[80]
	-	Centimeter-scale single- to few-layer G on Ni foils	Efficient roll-to-roll process	[81]
	-	N-doped graphene	N-type behavior useful to modulate G electrical properties	[82]
Electrochemical reduction of CO and CO_2	-	Several types of nanocarbons of controlled shape	Direct reaction of CO_2 with Mg metal	[83]
	-	G flakes	Room-temperature synthesis method on copper foil from different carbon sources using external charges	[84]
Arc discharge	-	Few-layered G	The reactivity of buffer gases (helium, oxygen-helium, and hydrogen-helium) is the key factor	[85]
	-	Few-layered G	Different mechanisms in the presence and absence of TiO_2 and ZnO catalysts	[86]
Unzipping carbon-nanotubes (CNT)	-	Chemical-free G	Radial and shear loading unzipping modes with cryomill method at 150 K	[70]
	-	G nanoribbons	Linear longitudinal opening of the Multi Wall CNT (MWCNT)	[87]
Organic synthesis	-	Two-dimensional G nanoribbons	Highly ordered monolayers (2D crystal) of larger G ribbons	[88]
Pyrolysis	-	General description	Pyrolysis of organic matter	[89]
	-	Metal-free catalyst of G sheets	Spray pyrolysis of iron carbonyl and pyridine	[90]
	-	G nanoporous with high specific surface area	Spray pyrolysis at different temperatures, graphene oxide-based precursor, nitrogen carrier gas	[91]

Table 2. Graphene synthesis with the top-down approach.

	Results		Highlight	Refs.
Mechanical	-	Monocrystalline graphitic films	Exfoliation of small mesas of highly oriented pyrolytic graphite	[42]
	-	G	Review: general description	[94]
	-	G sheets	Dispersion and exfoliation of graphite in N-methyl-pyrrolidone	[95]
	-	Stably single-layer G sheets in organic solvents	Exfoliation–reintercalation–expansion of graphite	[96]
	-	G nanoplatelet	Thin films on a low-density polyethylene substrate	[97]
Electrochemical expansion	-	Functional G sheets	Hyperexpanded graphite by electrolysis in a Li+ containing electrolyte and in situ electrochemical diazonium functionalization	[98]
	-	G flakes	Cathodic graphite expansion in dimethylformamide (DMF) and functionalization by reducing aryl diazonium salts in organic solution	[99]
	-	G	Exfoliation temperature increase from 25 to 95 °C reuslt in decrease of defects and increase of thermal stability (with H_2O_2 addition)	[100]
Chemical synthesis	-	G	Review: general description	[103]
	-	Carbon nanoscrolls	Low-temperature, catalyst-free graphite intercalation with alkali metals	[104]
	-	G and chemically modified G	From colloidal suspensions	[105]
Unzipping nanotube	-	Few-layer nanoribbons	Mechanical sonication and gas-phase oxidation in organic solvent of multiwalled carbon nanotubes	[106]
	-	G nanoribbons	Lengthwise cutting of MWCNTs by a solution-based oxidative process	[107]
	-	G nanoribbons	Plasma etching of CNT partly embedded in a polymer film	[108]
Microwave synthesis	-	Flower-like G on hexagonal boron nitride crystals (h-BN)	Microwave G growth on polymethyl methacrylate (PMMA)-coated h-BN flakes	[109] [110]
Chemical and/or thermal graphene oxide (GO) reduction	-	Polylactic acid (PLA)/rGO nanocomposites	Glucose and polhyvinilpyrrolidone (PVP) reduction of GO mixed with PLA	[111]
Reduction	-	rGO	Two different reducing mixed reagents: HI/NH and NH/HI. Review: 50 types of reducing agents	[114] [115]
	-	rGO		
Other	-	G	Review: different sizes and chemical compositions. Controlled segregation of G chemically modified on liquid interfaces	[116] [117]
	-	G networks		

The strong oxidation of graphite produces bulk solid graphite oxide that can be exfoliated in water or other suitable organic solvents to form GO [118–120]; several recent reviews report the synthesis of graphite oxide [121–123]. Graphite oxide can be prepared with Brodie [124], Staudenmaier [125], and Hummer's [126] methods. The synthetic technique and the extent of the reaction influence the degree of graphite oxidation; the most oxidized graphite oxide is produced with the Staudenmaier method, but this reaction may take several days. However, because both Staudenmaier and Brodie methods generate highly toxic ClO_2 gas that can decompose in air violently; thus, the most widely used method to prepare graphite oxide is Hummer's method.

With Hummer's method, the GO is prepared by exfoliating graphite oxide obtained from the oxidation of graphite powder with strong chemical oxidants, such as HNO_3, $KMnO_4$, and H_2SO_4 [112,113,126]. GO can be successively reduced to graphene by the partial restoration of the sp^2- hybridization by thermal [127], chemical [128], electrochemical [129], photothermal [130],

photocatalytic [69,131], sonochemical [132,133], and microwave reduction methods [134]. The high number of oxygen-containing groups of the obtained GO product permits the interaction with the cations, providing important reactive molecules for the nucleation and growth of nanoparticles and therefore the formation of various graphene-based composites.

3. The Photocatalytic Process: Fundamentals of Graphene-TiO_2 Photocatalysts

Photocatalysis is based on the activation of a semiconductor (SC) by the sun or artificial light. When an SC material is irradiated with photons whose energy is higher or equal to its band gap energy, a promotion of an electron from the valence band (VB) to the conduction band (CB) occurs with the concomitant generation of a hole in the valence band VB [135].

In a water system, oxygen adsorbed on the surface of the semiconductor acts as an electron acceptor, while the adsorbed water molecules and hydroxyl anions act as electron donors, leading to the formation of a very powerful oxidizing $^{\bullet}OH$ radical. The electrons react with oxygen molecules to form the superoxide anion, $O_2^{\bullet-}$. In the presence of a contaminant organic molecule (M), adsorbed on the catalyst surface, the $^{\bullet}OH$ radical is the primary oxidant that reacts to produce adducts, followed by the fragmentation of the molecular structure into several intermediates species until the total mineralization of contaminant is completed with the formation of CO_2 and H_2O [136–138].

The successful of photocatalytic process is therefore strictly dependent on the competition between the reaction of the electron with water on the SC surface and the electron-hole recombination process that releases heat or radiation.

The overall process can be described by the following reactions:

- $electron - hole\ pair\ generation$:

  $$SC + h\upsilon \rightarrow SC\left(e_{CB}^{-} + h_{VB}^{+}\right)$$
- $hydroxil\ radicals\ formation$:

  $$SC\left(h_{VB}^{+}\right) + H_2O_{ads} \rightarrow SC + {}^{\bullet}OH_{ads} + H_{ads}^{+}$$
- $superoxyde\ formation\ from\ electrons\ in\ CB\ and\ oxygen$:

  $$SC(e_{CB}^{-}) + O_{2\ ads} \rightarrow SC + O_{2ads}^{-}$$
- $adsorption\ of\ M\ on\ catalyst$:

  $$SC\left(h_{VB}^{+}\right) + M_{ads} \rightarrow SC + M_{ads}^{+}$$
- $the\ hydroxyl\ radical\ is\ the\ primary\ oxidant$:

  $$OH_{ads} + M_{ads} \rightarrow intermediate\ products \rightarrow CO_2 + H_2O$$

As an example, Khan et al. [23] defined the different intermediate degradation products of Methyl Orange by using TiO_2 photocatalysts that are resumed in Figure 2. The reported compounds are derived from the reaction of $^{\bullet}OH$ radicals with the final mineralization in CO_2 and water.

It is important to consider that, because the photocatalytic process is strictly dependent on the kinetics of charge carriers and redox reactions, the knowledge of the electronic processes that occur at the level of the SC surface are of great importance. In the SC, the oxidation fromphotogenerated holes and the reduction fromphotogenerated electrons may occur simultaneously and, to keep the photocatalyst electrically neutral, should occur at the same rate.

The photocatalytic activity is greatly limited by electron–hole recombination, and therefore several methods are used to increase the efficiency of charge carrier separation and therefore to improve the photocatalytic performance of the SC photocatalyst [139–141]. In this context, the combination of graphene with the SC photocatalyst represents an innovative strategy [55,69,142].

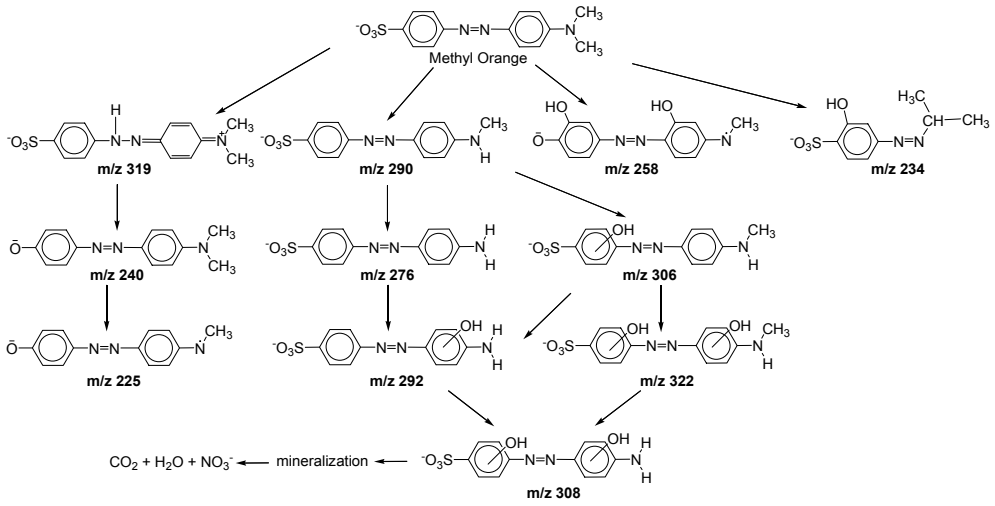

Figure 2. Proposed photodegradation mechanism of Methyl Orange [23].

Titanium dioxide (TiO2) is generally considered the best SC material that can be used as a photocatalyst [18,139,143], showing almost all of the required properties for an efficient photocatalytic process, except for activity under visible light irradiation.

From these considerations, TiO2/graphene nanocomposites ($GTiO_2Ns$) are widely used for photocatalytic applications, exploiting their potential in environmental applications.

The effective role of G in a photocatalytic event on $GTiO_2Ns$ has not been completely investigated, or is not completely understood. In order to explain the possible mechanism, the light source (UV or VIS light) and the presence/absence of dye molecules, or rather the presence of a compound able to absorb visible light, are fundamental.

When the target molecule does not adsorb light and is efficiently adsorbed on the photocatalyst surface:

(1) UV light excitation of $GTiO_2Ns$ photogenerates the electron–hole pairs and the electrons are then injected into graphene due to its more positive Fermi level [144]. This process is favored by the position of the work function of graphene that is −4.42 eV, with respect the conduction band of TiO_2 that is located at −4.20 eV [145]; from this consideration, the electron in the CB of TiO_2 is injected to G. Graphene scavengesphotogenerated electrons by dissolved oxygen; facilitates the hole-electron separation, reducing the recombination of e-(CB) and the holes (VB); and, due to its high carrier mobility, accelerates the electron transport, thus enhancing the photocatalytic performance [142,146].

(2) When the operational mechanism takes place via visible light, the electron transfer of thephotogenerated electron is promoted from the G photoexcited state and then delocalized to the TiO_2 surface. M.T Silva et al. indicated, by rGO photoluminescence study, that the photogenerated electrons under Vis or NIR laser can be transferred to the surface of TiO_2 with a consequent quenching of photoluminescence; also in this case, charge recombination is inhibited with a consequent increasing of photocatalytic activity under visible light [147]. It is important to know that the presence of G in $GTiO_2Ns$ photocatalyst produces a red shift in the absorption, reducing its band gap and thus extending the photoresponse to a longer wavelength [148]. The explanation of visible light activation in the $GTiO_2Ns$ composites is not clear, but it is possible to attribute this phenomena to the sensitization of TiO_2 due to the presence of graphene [147,149,150]. In this case, in the visible light excitation of $GTiO_2Ns$, graphene absorbs the light, and the photoexcited electrons in high energy G states are delocalized into the CB of the TiO_2 surface with the dissipation of excess energy due to electron vibrational interaction [151]; successively electrons

react with oxygen, resulting in the formation of superoxide radicals. In Figure 3, the activation mechanisms of $GTiO_2Ns$ under UV and visible light are reported.

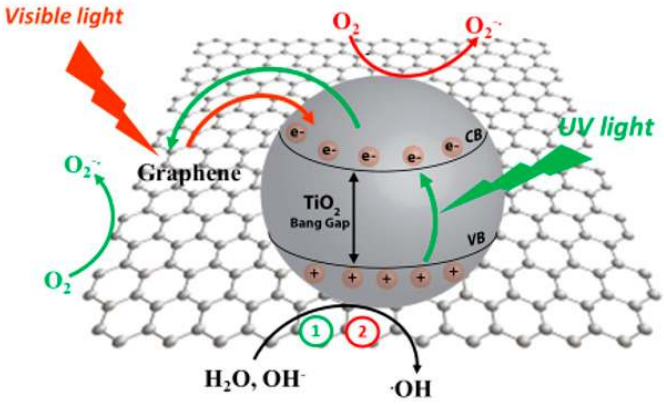

Figure 3. Mechanisms of UV and visible light activation of TiO_2 with G.

When a dye (D) as a target molecule is efficiently adsorbed onto the photocatalyst surface, the UV mechanism is the same as that reported before (1) while, under visible light, different activation pathways can be found. In this case, the dye acts both as a sensitizer for visible-activation and as a pollutant during the photocatalytic process, promoting the electron transfer from the excited dye molecules state to the TiO_2 CB while G acts as an electron scavenger, as in the UV mechanism [147].

The other possible pathway under visible light involves G which acts as visible light sensitizer promoting the electron transfer to the TiO_2 CB (as in 2) [152–154] (Figure 4). This process is less probable due to the competition between G and D as light sensitizers, but in any case is possible.

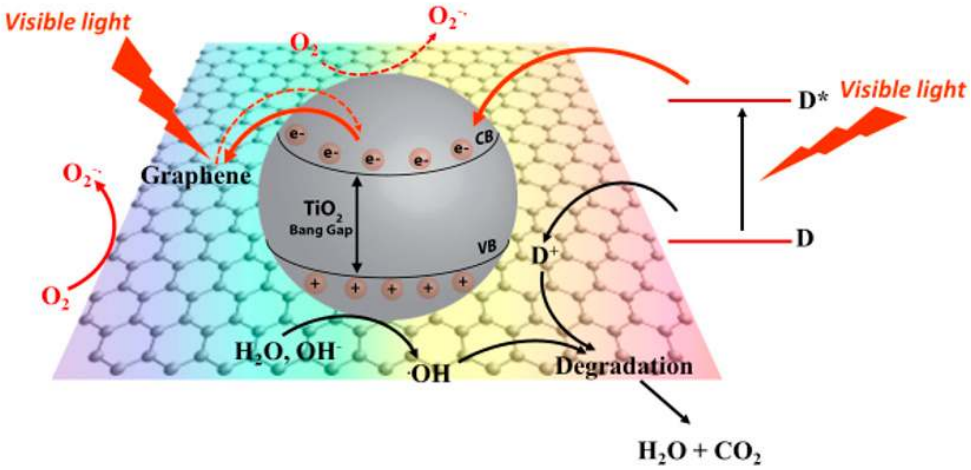

Figure 4. Mechanisms of UV and visible light activation of TiO_2 with G in the presence of dye (D).

4. Preparation Methods of $GTiO_2Ns$

According to the facts that graphene doping of TiO_2 generally contributes to the bathochromic shift of the absorption band, hinders the recombination of h^+/e^- by transferring the photoexcited electron to the graphene surface, which also enhances the surface area of TiO_2 for better adsorptive properties [155], the investigation of $GTiO_2Ns$ photoactivity under visible light seems to be crucial. The improvement of performance due to the presence of G in $GTiO_2Ns$ photocatalyst is primarily attributed to the extension of the light absorption range, the increase of absorptivity, and the efficient charge separation and transportation. With $GTiO_2Ns$ photocatalyst, the rate of h^+/e^- recombination

after light excitation decreases [156], while the charge transfer rate of electrons increases in addition to the surface-adsorption of chemical species thanks to π-π interactions [157].

However, the properties $GTiO_2Ns$ and different operational parameters, such as the characteristics of substrates, UV-vis or Vis light irradiation, etc., can affect the photocatalytic efficiency [157].

$GTiO_2Ns$ can be generally categorized into three kinds: TiO_2-mounted activated graphene [92], graphene-doped TiO_2, and graphene-coated TiO_2 [158]. Each of these types exhibits good photocatalytic activity. In order to improve the efficiency, the surface properties of graphene could be adjusted via chemical modification, which facilitates its use in composite materials [156,159,160].

$GTiO_2Ns$ can be generally realized in two different ways by "ex situ hybridization" or "in situ crystallization". In Figure 5, a schematic representation of ex situ hybridization and in situ crystallization in the synthesis of $GTiO_2NPs$ is reported.

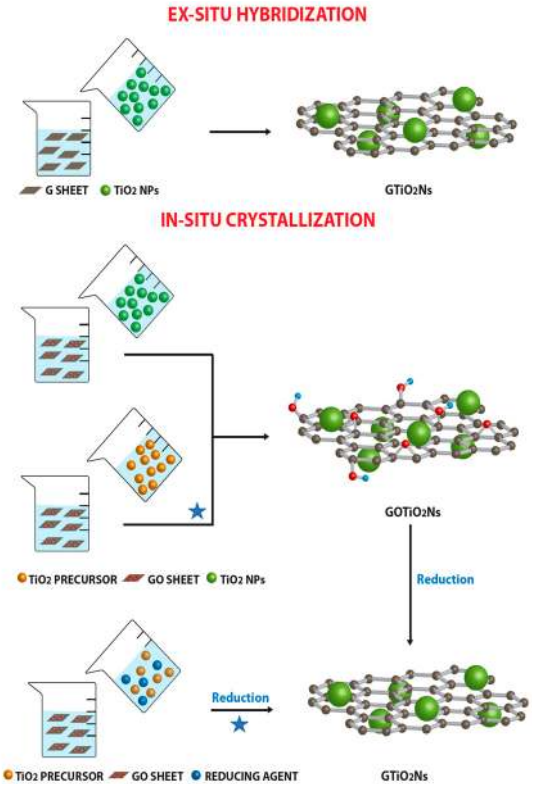

Figure 5. Schematic representation of ex situ hybridization and in situ crystallization in the synthesis of $GTiO_2Ns$.

Ex situ hybridization (Table 3) involves the mixing of graphene dispersions with pre-synthesized TiO_2 nanoparticles (TiO_2NPs) [147]. To enhance their solubility and improve the quality of $GTiO_2Ns$ composites, before mixing, TiO_2NPs and/or graphene sheets can be functionalized by covalent C–C coupling [59,161] or non-covalent π-π stacking reactions [162]. For example, Morawski et al. [163] prepared a visible light-active TiO_2-reduced GO photocatalyst by mechanically mixing TiO_2 with an appropriate mass ratio of reduced GO in 1-butyl alcohol and successive ultrasonication. Yong Liu et al. [164] prepared a graphene aqueous dispersion by sonicating a mixture of graphene raw materials with polyvinylpyrrolidone (PVP) as surfactant and a suspension of TiO_2 by dispersing TiO_2 powder in deionized water with ultrasonication. In this preparation, graphene-TiO_2 composite material was obtained by simple mechanical mixing and sonication using anhydrous ethanol to improve the wettability of the dispersion, while spray-coating was carried out both on polycarbonate and on rubber substrates to facilitate the testing of photocatalytic performance. Ramesh Raliya et al. [165] also

prepared nanomaterial/composite solutions by mixing GO at different concentration ratios to TiO_2 and tested their effects on photocatalytic performance.

However, with ex situ hybridization, in some cases it is possible to obtain a low-density and non-uniform coverage of nanostructures by G sheets [113,166–169].

The most common strategy to synthetize $GTiO_2Ns$ nanocomposites is represented by *in situ crystallization* (Table 3). In this case, GO or rGO are usually used as starting materials for the presence of oxygen-containing functional groups on their surface. In fact, they act as a nucleation point for grooving and anchoring semiconductor nanocrystals. The successive reduction of GO generates $GTiO_2Ns$ with homogeneous distribution on 2D nanosheets, thereby promoting the direct interaction between semiconductor nanocrystals and G. For this reason, various methods, such as mixing, hydrothermal/solvothermal methods, sol-gel, electrochemical deposition, combustion, microwave, photo-assisted reduction, and self-assemble approaches, can be applied for the synthesis of $GTiO_2Ns$ [66,170,171].

In the *mixing method* (M), GO and semiconductors are mixed with stirring and ultrasonication in order to obtain the exfoliation of GO and, successively, GO/TiO_2 product with uniform distribution; in a second step the reduction of GO is performed [51,172–175].

A strong mixing and the best chemical interaction between GO and TiO_2 can be obtained by applying the sol-gel method (SG). As an example, Zhang et al. [176] used a sol-gel method to prepare a series of TiO_2 and graphene sheet composites by using tetrabutyl titanate and graphite oxide and the obtained precursors were calcinated at 450 °C for 2 h under air or nitrogen atmospheres. Zabihi et al. [177] prepared photocatalytic composite thin films of $GTiO_2Ns$ with a low-temperature synthetic process by using G dispersion and titanium isopropoxide bis (acetylacetonate) solution by using a sol-gel chemical method. Spin- and spray-coating was successively used for films deposition; the use of ultrasonic vibration demonstrated a positive effect from both sol-gel and deposition processes that produced rutile and anatase nanoparticles inclused in a matrix of few-layered graphene thin film.

Gopalakrishnan et al. [178] prepared TiO_2-reduced GO nanocomposites in situ from the incorporation of TiO_2 sol into GO sheets and the successive solvothermal method without the addiction of any chemicals. Shao et al. [179] reported a novel so-called gel-sol process for the synthesis of TiO_2 nanorods combining rGO composites by utilizing the triethanolamine as a shape controller and under specific conditions. The as-fabricated hybrid composites presented distinct advantages over the traditional methods in terms of the well-confined TiO_2 morphology and the formation of Ti-C bonds between TiO_2 nanoroads and rGO simultaneously. Long et al. [180] used the hydrothermal method to prepare efficient visible light active $GTiO_2Ns$ by using a GO suspension and TiO_2 sol with undergrown TiO_2 nanoparticles at 413 K. The study of obtained materials demonstrated high chemical interaction at the interface of GO sheets and the polymeric Ti-O-Ti structure that facilitated the retaining of more alkoxyl groups; the induced crystal disorders and oxygen vacancies contributed positively to the performance of the obtained photocatalyst.

In the *hydrothermal/solvothermal methods* (HD/SD), semiconductor nanoparticles or their precursors are loaded on GO sheets that are successively reduced to rGO involving reactions under controlled temperature and or pressure. For example, Hao Zhang et al. [181] obtained a $GTiO_2Ns$ (P25) nanocomposite photocatalyst with a high adsorptivity of dyes and a greater light absorption range by using a one-step hydrothermal reaction obtaining both GO reduction and P25 cover. Hu et al. [182] successfully synthesized different structures of TiO_2-graphene composites through the hydrothermal reaction by using GO and different titanium sources in hydrothermal conditions. The results showed the larger interfacial contact between TiO_2 and G, in addition to the greater surface area of the poriferous composite. Hamandi et al. [183] studied the influence of the photocatalytic performance of TiO_2 nanotubes (NT) resulting from the addition of GO. TiO_2 nanotubes were prepared using alkaline hydrothermal treatment of TiO_2 P25 followed by calcination at 400 °C under air, while GO-NT composites were obtained by the wet impregnation of the as-prepared TiO_2 nanotubes onto graphene oxide before reduction under H_2 at 200 °C. Sijia et al. [184] synthesized a novel composite photocatalyst,

reduced graphene oxide (rGO)-modified superlong TiO_2 nanotubes with a length of about 500 nm, by an improved hydrothermal process and a heating reflux method.

A hybrid nanocomposite containing nanocrystalline TiO_2 and graphene-related materials (GO and rGO) was prepared from Kusiak et al. [185] by using the hydrothermal method under elevated pressure. In this preparation, the presence of graphitic carbon depends on temperature, the type of modification method, and the preparation conditions, obtaining multilayer GO flakes in comparison to rGO flakes. This multilayer character produced the most intensive time resolved microwave conductivity signals under both UV and visible illumination for materials modified with GO, indicating that more electrons are induced in the conduction band of hybrid nanocomposites. Li et al. [186] synthesized reduced graphene oxide-TiO_2 (rGO-TiO_2) composites with a sandwich-like structure by using a simple solvothermal method. Hemraj et al. [187] synthesized nanocrystalline anatase TiO_2-GO nanocomposites by two steps with the initial preparation of anatase TiO_2NPs by a simple sol-gel method and the successive decoration of GO on its surface by using a facile solvothermal method. Ju Hu et al. [188] synthesized TiO_2/reduced graphene oxide nanocomposites by using a one-step surfactant-assisted hydrothermal method. Compared with the control TiO_2/rGO nanocomposite, TiO_2/rGO-X (X = sodium dodecyl benzene sulfonate, Triton X-100, and acetyl trimethyl ammonium bromide) presented excellent photocatalytic activity. The study indicated that the surfactant-assisted hydrothermal method is an effective approach to improve the structure, morphology, and photocatalytic performance of TiO_2/rGO composites.

Semiconductor nanostructures can be *electrolytically deposited* on the surface of graphene-based substrates, at low temperature condition, from an aqueous solution containing the semiconductor. For example, Ming-Zheng Ge et al. [189] adopted both electrodeposition and carbonation methods to deposit rGO films on TiO_2 nanotubes obtained with two-step electrochemical anodization. Recently, Guimaraes de Oliveira et al. [190] used the electrochemical method to deposite GTiO_2Ns composite film on a Ti substrate by using GO and Ti(IV) aqueous solution, demonstrating a photocatalytic activity almost twice as high as that observed for the TiO_2 only film.

The *microwave-assisted strategy*, in this context, addresses the synthesis of semiconductor nanomaterials of a controlled size and shape. For example, Shanmugama et al. [191] synthesized GTiO_2Ns nanocomposites by a novel surfactant-free, environmentally friendly one-pot in situ microwave method. This method leads to the uniform distribution of TiO_2 nanoparticles on G sheets with the binding nature of TiO_2. Wang et al. [192] reduced GO with both direct and microwave-assisted reduction in the presence of Ti powders, showing that the microwave effect decreased the reduction time. In this case, Ti ions derived from the reaction of Ti powder with GO were hydrolytically transferred to TiO_2 with the formation of rGO-TiO_2, which was proven to be an active material in the removal of methylene blue. Yang et al. [193] prepared nanocomposites of TiO_2 and rGO, with a fast and simple microwave irradiation method by the reaction of graphene-oxide and commercial TiO_2 nanoparticles in water/ethanol solvent, examining different microwave powers with different time intervals. The effect of time and power on absorption wavelength and the creation of defects in the graphene layer was examined, obtaining an optimum irradiation time in which the nanocomposite presented the highest absorption wavelength (the smallest band gap), and the optimum value for microwave power in which the nanocomposite had the lowest number of defects. First, GO was prepared using a modified Hummer's method, and then TiO_2 and the mixture of water/ethanol and graphene-oxide (GO) was used for the hydrolysis of TiO_2, followed by its mounting on graphene-oxide. In this way, microwave irradiation reduced GO to graphene with the formation of TiO_2/rGO nanocomposites.

Other methods have been investigated, such as that proposed by Pu et al. [194] regarding the synthesis of TiO_2-rGO nanocomposites, conducted simultaneously with the *photoreduction* (PR) of GO nanosheets in a simple GO and TiO_2 ethanol system, demonstrating a facile and environmentally friendly strategy for the in situ preparation of the TiO_2-rGO hybrid "dyade". In Table 3, the principal synthesis methods of GTiO_2Ns are summarized.

Table 3. The synthesis methods of Graphene Based TiO_2 nanocomposites.

Photocatalyst	Synthetic Route	Starting Graphite	Starting Semiconductor	Refs.
Ex-Situ Hybridization				
rGO/TiO_2	Mechanical mixing and ultrasonication	rGO	TiO_2NPs in 1-butyl alcohol	[163]
G/TiO_2	Mechanical mixing and ultrasonication	G in PVP/water	TiO_2NPs anatase in water	[164]
GO/TiO_2	Mechanical mixing	GO	Titanium isopropoxide	[165]
In-Situ Crystallization				
rGO/TiO_2	M with GO and PR reduction	GO	TiO_2NPs	[174]
	M and GO and ST reduction	GO	TiO_2NPs	[175]
G/TiO_2	ST	GO	Tetrabutyl titanate	[145]
G/TiO_2	SG	rGO	Titanium isopropoxide	[146]
G/TiO_2	HD	GO	P25	[147]
rGO/TiO_2	SG	GO	Tetrabutyl titanate	[176]
G/TiO_2	SG	G dispersion	Titanium isopropoxide	[177]
rGO/TiO_2	Solvothermal SG	GO sheets	TiO_2 sol	[178]
rGO/TiO_2	SG	GO	Titanium isopropoxide	[179]
G/TiO_2	HD	GO suspension	TiO_2 sol	[180]
G/TiO_2	one-step HD	GO water/ethanol	TiO_2	[181]
G/TiO_2	HD	GO	Different Ti sources	[182]
G/TiO_2	Wet impregnation and thermal reduction (H_2)	GO	TiO_2 nanotubes from *HD* of TiO_2 P25	[183]
rGO superlong TiO_2	HD and heating reflux	GO	Super long TiO_2	[184]
GO and rGO/TiO_2 (nanocristals)	Elevated pressure HD	GO and rGO	TiO_2	[185]
rGO/TiO_2 sandwich-like structure	HD/ST	rGO	Butyl titanate	[186]
nanocrystalline anatase TiO_2-GO	SG and GO decoration by ST	GO	Anatase TiO_2NPs by *SG*	[187]
TiO_2/rGO-X nanocomposites	One-step surfactant (X)-assisted HD	GO	TiO_2 (P25)	[188]
rGO films on TiO_2 nanotubes	Two-step ED and carbonation techniques	rGO	Two-step anodized TiO_2 nanotubes from Ti foils	[189]
Ti plate deposited TiO_2 and GO film	ED	GO from nanographite	Ti plate and K_2TiF_6 aqueous solution	[190]
G/TiO_2	MW	GO	$TiCl_4$	[191]
rGO/TiO_2	MW	GO	Ti powder	[192]
rGO/TiO_2	MW	GO	TiO_2NPs	[193]
rGO/TiO_2	PR	GO	TiO_2NPs	[194]
rGO/TiO2	PR	GO	Colloidal TiO_2	[156]

5. Photocatalytic Degradation of Dyes with GTiO_2Ns

Dye molecules, which are solubilized during several application processes, present different colors derived from the selective absorption of light. Coloring properties of dyes depend on their chemical structure consisting of two fundamental components: the chromophore and the auxochrome. The chromophore is a covalently unsaturated group, which is responsible for the color production

for the absorption in the UV or visible region; the auxochrome is supplementary to the chromophore, and influences the solubility in water and the affinity towards a particular support [195]. Concerning their uses, dyes can be anionic, cationic, and non-ionic; anionic dyes are divided into direct, acid, and reactive dyes, while cationic dyes are basic [196]. Water treatments by using $GTiO_2Ns$ in the photocatalytic degradations of dyes became very important due to the danger of dyes as environmental pollutants [142].

Methylene blue (MB) was first prepared by Caro in 1876 as an aniline-derived dye for textiles, and is largely used as a water-soluble cationic dye in the dyeing of paper, wood, plastic, silk, and cotton, as well as in scientific research and pharmaceutical industries [197,198]. Kyeong Min Cho et al. [8], to obtain MB photodegradation, used hydrothermal methods in the self-assembly of TiO_2 precursors, GO, and a surfactant to prepare rGO mesoporous TiO_2; this material showed high photocatalytic performances in the MB degradation test, good ability in the charge separation, and a large surface area compared to typical $GTiO_2Ns$.

Hanan H. Mohamed [199] recently described the simultaneous photoassisted oxidation of MB by using new synthesized hierarchical structures of anatase/rutile TiO_2 microsphere-rGO nanocomposites. Interestingly, rutile/anatase phase transformation was observed upon changing the GO content. The synthesized nanocomposites showed enhanced photocatalytic activity for the dye degradation compared to pristine TiO_2 nanoparticles that was attributed to the synergetic effect between anatase and rutile in the synthesized TiO_2 microsphere composites. Also, Zhang et al. [200] synthesized graphene-supported mesoporous titania nanosheets ($GTiO_2Ns$) by using liquid-phase exfoliated G as a template and sandwich-like G-silica as intermediates. $GTiO_2Ns$ showed a mesoporous structure formed by crystalline TiO_2 nanoparticles anchored on G nanosheets that showed high surface areas. These characteristics significantly enhanced the photocatalytic activity of TiO_2 in the MB degradation.

Najafi et al. [201] fabricated TiO_2-GO nanocomposites with different nanowire and nanoparticle morphologies of TiO_2 by using a one-step hydrothermal method. The different morphologies of TiO_2 were grown on the surface of the GO sheets, previously synthesized by the modified Hummer's method. The obtained TiO_2-GO nanocomposites showed a tetragonal structure and covalent bonds between TiO_2 nanostructures and GO sheets. The best photodegradation rate of MB was found by using TiO_2 nanowire-GO nanocomposites. Divya et al. [202] used microwave irradiation of different GO weights and tetrabutyl titanate in isopropyl alcohol to obtain TiO_2 hybridation with the formation of $GTiO_2Ns$ nanocomposites. In this method, the irradiation with microwaves increase the temperature in a short time, favoring the GO reduction to G and the growth of TiO_2 nanoparticles on the G surface. The obtained $GTiO_2Ns$ nanocomposites presented efficient electron conductivity in G, therefore showing a reduced electron-hole recombination rate.

Another example is that of Sohail et al. [203], who prepared GO nanosheets by using a modified Hummer's technique with the successive conversion into particles by a spray-drying method. TiO_2 nanoparticles were grown on the surface of GO particles to obtain rGO-TiO_2 nanocomposites that showed better photocatalytic activities upon the degradation of MB compared to pure TiO_2, also showing in this case that rGO played an important role in the charge recombination to enhance the electron-hole separation.

Tseng et al. [204] studied a facile process to fabricate two-dimensional titania nanosheets (t-NS) by using GO as a support with in situ growth of anatase TiO_2 on GO suspended in butanol by combining the sol-gel and solvothermal processes without further calcination. Significant amounts of MB molecules can easily be adsorbed on the intrinsic graphitic structure. An optimum rate of hole titration by ethylenediaminetetraacetic acid was essential to efficiently reduce the recombination of charge carriers and consequently produce more active radicals to decompose MB. The strong interaction between graphitic and titania structures, rather than the crystallite size of anatase, dominated the photoreduction capability of t-NS.

Similarly, Minella et al. [205] obtained rGO-TiO_2 and rGO-SiO_2 hybrid materials by reducing different quantities of GO with hydrazine in the presence of TiO_2 and SiO_2 nanoparticles;

the photocatalytic activity of these nanomaterials was evaluated in the degradation of MB under both UV-vis and only visible light irradiation. The results showed that MB was strongly adsorbed on these new materials with an increase of degradation rates with respect to pristine semiconductors. The visible light degradation of MB was attributed to the dye-sensitization mechanism, while the UV-vis degradation was considered to be the typical semiconductor photocatalytic mechanism.

"Biphasic TiO_2 nanoparticles" and their G nanocomposites were synthesized by Raja et al. [206] by the hydrothermal method. Introducing high surface area, G suppressed the electron-hole pair recombination rate in the nanocomposites. Further, the nanocomposites showed a red-shift of the absorption edge with a contraction of the band gap from 2.98 eV to 2.85 eV. The characterization of photocatalytic activities under natural sunlight and UV-filtered sunlight irradiation revealed that the $GTiO_2Ns$ composite exhibited about a 15- and 3.5-fold increase in the degradability of Congo red and MB dyes, respectively, in comparison to pristine TiO_2. The authors therefore developed a visible light active G composite catalyst that can degrade both cationic and anionic dyes, making it potentially useful in environmental remediation and water splitting applications under direct sunlight.

The ex situ hydrothermal method was proposed from Verma et al. [207] to synthesize rGO mixed TiO_2 nano-composites. The study demonstrated that the cooperation between the optimal phase ratio of TiO_2 (anatase/rutile) and rGO produced a positive system in the photocatalytic degradation test with MB other than antibacterial activity. Atchudan et al. [208] used a solvothermal method to prepare GO grafting TiO_2 nanocomposites and studied it as a photoactive material under UV-light irradiation in the degradation of MB and methyl orange. The obtained degradation efficiency, compared with only TiO_2, demonstrated the important function that GO played in the increase of performance due to the increase of light absorption and reducing charge recombination.

Darvishi et al. [209] instead used titanium butoxide (TBO) as a TiO_2 precursor, commercial TiO_2, and GO in a water/ethanol mixture to produce hydrolytically, and under microwave irradiation, rGO-TiO_2 nanocomposites; these showed high conductive and light absorption properties, demonstrating an enhancement of photocatalytic MB degradation. In these nanocomposites, the content of G improved the photocatalytic performances of the photocatalysts.

An example of an eco-friendly method was studied by Rezaei et al. [210], who synthesized TiO_2-graphene nanocomposites by the addition of the "blackberry juice" to GO as a reducing agent to produce rGO nano-sheets. The obtained TiO_2 (anatase)-rGO materials exhibited an excellent photocatalytic activity toward MB degradation due to the enlarged surface area and the collaborative effect of rGO. Shanmugam et al. [191] synthesized $GTiO_2Ns$ nanocomposites by a surfactant-free, environmentally friendly one-pot in situ microwave method. TiO_2 nanoparticles of 5–10 nm were distributed on the G sheets. The photocatalytic activity of pure TiO_2 and $GTiO_2Ns$ nanocomposites was studied under UV and visible light irradiation sources with MB. The studies revealed the highest degradation efficiency of 97% with UV light and 96% with visible light irradiation by using the $GTiO_2Ns$ photocatalyst, opening the possibility of using this material for industrial wastewater treatment.

The sol-gel technique was used by Rezaei [211], who prepared GO-TiO_2 nanocomposites by evaluating the photocatalytic activities of MB aqueous solution under sunlight irradiation. The results showed that the nanocomposite containing 9.0 wt % of GO had the highest photocatalytic performance in the MB degradation to either "single-phase anatase" or other composites containing different GO quantities. The improvement of the photocatalytic activity was attributed to the favorable effect of the distribution of TiO_2 nanoparticles of less than 20 nm on GO sheets.

UV-assisted photocatalytic reduction of GO by TiO_2 nanoparticles in ethanol was used by Charoensuk et al. [212] in the preparation of rGO-TiO_2 nanocomposites. The photocatalytic activity of prepared rGO/TiO_2 and GO/TiO_2 nanocomposites was evaluated by the kinetics of the photocatalytic degradation of MB under UV irradiation. Significant roles in the MB photodegradation were played by important factors such as the bandgap, electron-hole recombination, characteristics of surface (area and functional groups), and adsorption capacity of nanocomposites. The results revealed that

rGO/TiO_2 and GO/TiO_2 nanocomposites exhibited efficient charge separation, showing about 500% improvement of photocatalytic activity in MB photodegradation compared to pristine TiO_2.

The solvothermal technique was used by Wang et al. [213], who prepared an efficient photocatalyst of nano TiO_2-functionalized GO nanocomposites. This nanomaterial showed an quadruple increase in MB photodegradation activity with respect to that obtained by using the P25-graphene composite photocatalyst. Liu et al. [214] instead used an interesting impregnation-hydrothermal method to prepare highly distributed TiO_2 nanoparticles with in situ growth on functional G (FG), which was before obtained by modifying GO by using triethanolamine. The obtained FGTiO_2Ns photocatalyst showed better photocatalytic activity under UV light irradiation with respect to pure TiO_2 and GO-TiO_2 prepared by other similar methods, also revealing considerable photocatalytic skill under visible light irradiation.

A fruitful method to produce expanded exfoliated GO (EGO) was used by Baldissarelli et al. [215]. The use of ozone exposure and thermal treatment transformated the graphite surface to a G-like surface containing oxygen and sp^3 carbon. The EGO, obtained through thermal treatment, produced, with the addition of TiO_2 nanoparticles, photocatalytic TiO_2-EGO nanocomposites that demonstrated higher activity with respect to that produced by the common Hummer's method. In particular, TiO_2-EGO showed enhanced MB photodegradation under UV light compared to TiO_2 P25.

A new nanomaterial composed of ultrasmall TiO_2 nanoparticles and rGO nanosheets was prepared by Gu et al. [216], who used glucosamine in alkaline conditions under hydrothermal treatment. In this synthesis, glucosamine regulated the growth and homogeneity of TiO_2 nanoparticles dispersed on the G structure, permitting the formation of the expected GTiO_2Ns products, demonstrating that TiO_2 nanoparticles about 13 nm in diameter were strongly anchored on G. Different GTiO_2Ns samples were calcined at several temperatures; in particular, the GTiO_2Ns sample treated at 700 °C showed good photocatalytic activity in MB photodegradation compared to those produced at other calcination temperatures.

Moreover, Fan et al. [217] used the hydrothermal method to synthesize TiO_2 nanospindles, which are featured by large exposed {0 0 1} facets, and then fabricated TiO_2 nanospindles/reduced GO nanocomposites (rGO-TiO_2). The photocatalytic activity in the photodegradation of MB showed an impressive photocatalytic enhancement of rGO-TiO_2 with respect to pure TiO_2 nanospindles. In addition, Sun et al. [218] used a one-step in situ hydrothermal method to prepare chemically bonded GTiO_2 nanorods hybrid composites with high dispersity by using GO and TiO_2 (P25) as the starting materials without using reducing agents. Ultraviolet-visible diffuse reflectance measurements of the composites showed an enhanced light absorption and a red shift of absorption edge. When GTiO_2Ns nanorods hybrid composites were used as photocatalysts, they showed an enhancement of photocatalytic performance in the photodegradation of MB under visible light irradiation compared to that of pristine TiO_2 nanorods.

Rong et al. [219] prepared different GTiO_2Ns photocatalysts with a simple hydrothermal method. First, GO (obtained from graphite oxidation) was dispersed in a water/ethanol solution with ultrasonic treatment, after which TiO_2 was added and a thermal treatment at 120° for 12 h was used. A series of GTiO_2Ns photocatalysts obtained with different oxidation times (in the GO production from graphite) and GO contents were obtained. When these materials were applied to the photodegradation of MB under visible light irradiation, they exhibited excellent photocatalytic activities.

Gupta et al. [220] proposed a strategy to fabricate G quantum dots (GQDs) infilled TiO_2 nanotube arrays hybrid structure (GQDs-TiO_2NTAs) for the application of MB degradation under UV light irradiation. In particular, anodic oxidation of a Ti sheet by using an impregnation method produced the fill of GQDs into TiO_2 NTAs. The application of this material in the adsorption and photodegradation of MB in an aqueous solution under UV light irradiation showed high photocatalytic efficiency, which was attributed to the favorable visible light absorption and to efficiency in the transfer of photogenerated electrons from the TiO_2NTAs to GQDs that produced large photoinduced charge separation. No less important was the strong adsorption capacity of the GQDs to MB molecules.

GP-wrapped TiO_2 ($GwTiO_2$) hybrid material was fabricated by Ni et al. [221] with the simultaneous reduction and wrapping of GO on the surface of high-reactive anatase TiO_2, based on the surface negatively charged property of GO. $GwTiO_2$ gave a strong red-shifted light absorption edge and a contracted bandgap compared to that of GP randomly supported TiO_2; this behavior was attributed to the positive chemical interaction between TiO_2 and G. The photocatalytic MB degradation under a xenon lamp and visible light irradiation confirmed the best quality of this nanomaterial. Furthermore, Yang et al. [222] prepared TiO_2/G porous composites with rGO by using a template of G microsphere colloidal crystals that showed high light absorbing properties, and good MB adsorption properties, other than a fast ability in the charge transportation and separation. These porous composites showed high degradation activities in MB degradation under visible light irradiation with a constant rate almost 6.5 times higher than that of P25 under the same conditions.

Also, Suave et al. [223] prepared photocatalytic TiO_2 nanocomposites with different loads of ozonated graphene (OGn) and evaluated the performances in photocatalytic MB degradation and other dyes using UVC irradiation. Although the photocatalytic activity decreased with each cycle, it is possible to reuse the nanocomposite that facilitates its practical application for water treatment.

In Table 4, the different preparation methods of $GTiO_2Ns$ applied to MB photodegradation are listed.

Table 4. Photocatalytic applications of Graphene Based TiO_2 nanocomposites in the degradation of Methylene Blue.

Photoactive Nanomaterials	Dye Conc. (mg/L)	Catalyst Quantity (g/L)	Light Source	Irradiation Time (min)	Degradation (%)	Refs.
G/TiO_2	9.60	0.33	Visible	180	90	[8]
P25-G	8.64	0.6	UV	60	85	[199]
P25-G	8.64	0.6	Visible	60	65	[199]
G/TiO_2	10	0.6	UV	120	100	[200]
G/TiO_2	10	0.2	UV	40	85	[202]
TiO_2@rGO	–	0.1	UV	120	92	[203]
GO/TiO_2	15	0.2	UV	350	92	[204]
TiO_2-G	0.13	0.5	UV-Vis	450	100	[205]
rGO/TiO_2	320	0.5	Visible	90	95	[207]
TiO_2/GO	–	0.2	UV	25	100	[208]
TiO_2/G	0.13	0.4	UV	60	96	[209]
TiO_2/G	3	0.48	Visible	90	100	[210]
G/TiO_2	3.2	0.2	UV	180	97	[191]
G/TiO_2	3.2	0.2	Visible	240	96	[191]
TiO_2/GO	3	0.48	Visible	60	94	[211]
TiO_2/GO	5	0.1	UV	40	93	[213]
TiO_2/GO	5	0.1	Visible	40	70	[213]
TiO_2-Graphite Oxide	10	0.5	UV	60	100	[215]
TiO_2/G	10	0.2	UV	20	97	[216]
TiO_2/rGO	10	0.17	UV	60	100	[217]
G/TiO_2	5	0.5	Visible	100	70	[218]
TiO_2/G	10	0.8	Visible	100	98.8	[219]
Graphene quantum dots/TiO_2	6.4	–	UV	180	100	[220]
TiO_2/GO	10	0.1	UV	180	100	[221]
TiO_2/G	10	0.01	Visible	150	100	[222]
TiO_2/G	10	0.5	UV	90	100	[223]
Graphene quantum dots/TiO_2	6.4	–	UV	180	100	[220]

Methyl orange (MO) is a well-known anionic azo dye largely used in the textile, printing, paper, food, pharmaceutical, and research fields [224]. As an example, MO photodegradation was studied by Lavanya et al. [225], who combined novel reduced graphene oxide (rGO) with anatase/rutile mixed phase TiO_2 nanofibers (MPTNFs), by using electrospinning and easy chemical methods, to enhance the photocatalytic performance. The photocatalytic activity in the photodegradation of MO showed a significant increase in the reaction rate for the synergistic effect of anatase/rutile mixed phase in one-dimensional nanostructures, and the electronic interaction between TiO_2 and rGO that provided

the improvement of electron transfer reduced the charge recombination for the enhancement of catalytic efficiency.

Xu et al. [63] used a two-step method to prepare G-pasted TiO_2 spheres. In the first step, the total cover of the surface of TiO_2 spheres with small GO sheets was obtained, while in the second step, GO was photocatalytically reducted in situ. G-pasted TiO_2 spheres presented more interfaces between G and TiO_2 with favorable interaction under the light irradiation compared to that of typical GTiO_2Ns composites. As a result, these materials demonstrated higher photocatalytic activity in MO degradation. Hou et al. [226] instead used hydrothermal synthesis to obtain rGO-TiO_2 composites, and part of these were successively calcined at 450 °C (CS-rGO-TiO_2). Photocatalytic activities in the decomposition of MO under UV, visible, and solar light by using both RGO-TiO_2 and calcinated composites were tested. The amount of G apparently influenced the photocatalytic activities of both rGO-TiO_2 composites and CS-rGO-TiO_2, which showed better photocatalytic activity compared to that of rGO-TiO_2. These results were due to the calcination that favored the oxidation of residual organics in the rGO-TiO_2 and a better crystallization of TiO_2 nanoparticles with smaller diameters.

Zhao et al. [227] synthetized three-dimensional nanocomposites with TiO_2 nanotubes (TNTs) and rGO nanosheets by using the hydrothermal method. The obtained rGO/TNTs nanocomposites presented sufficient active sites and gave the path of good electron-transport. These nanomaterials showed better photocatalytic activity in MO degradation under UV-light irradiation with respect to traditional TiO_2 nanotubes. Also, Lu et al. [228] combined TiO_2 and GO and used UV irradiation to synthesize rGO-TiO_2 composites. The influence of TiO_2 quantity and UV irradiation time on the rGO formation during the composite synthesis was investigated. The results demonstrated that a longer UV irradiation time corresponded to a higher reduction degree of GO, and therefore to a higher photodegradation efficiency of the composites in MO photodegradation. However, the results also showed that excessive UV irradiation times gave a negative effect on the photodegradation efficiency and therefore proposed a mechanism that correlated the reduction degree of GO with the photodegradation efficiency of composites.

Chemisorption and successive heating at different temperatures was applied by Xia et al. [229] to combine TiO_2 in different anatase and rutile phases with G sheets. The photoactivities of these nanomaterials were tested by using MO under UV and visible light irradiation, demonstrating an enhanced respect to only TiO_2. Notably, the different crystallite phases of TiO_2 reacted with different behaviors under UV and visible light irradiation due to the different charge transfer mechanisms.

Another example was described by Ge et al. [230], who combined electrodeposition and carbonation techniques to obtain the deposition of rGO films on TiO_2 nanotube arrays (TiO_2 NTAs); these materials, prepared in ethylene glycol by using two-step electrochemical anodization, showed an enhanced MO photocatalytic degradation with respect to both pristine TiO_2 NTAs and annealed TiO_2 NTAs under the same conditions. The increase of efficiency in photocatalytic degradation was due to the increase of separation efficiency of photoinduced electrons and holes, to red-shift in the UV absorption and to the profitable adsorbent skill of rGO towards the MO dye.

GTiO_2Ns nanocomposites were instead synthetized by Han et al. [231] by using the hydrothermal method and a successive annealing process. In this preparation, the loading of flocculent-like TiO_2 nanostructures onto G sheets was obtained. The evaluation of photoelectrochemical activities and the photocatalytic degradation of MO under UV light irradiation showed that the flocculent-like GTiO_2Ns composites presented the greatest photocatalytic activity compared to that of commercial anatase TiO_2, due to the increase of light absorption and fruitful charge separation of the nanocomposite structure.

In order to synthesize rGO wrapped with anatase mesoporous TiO_2 nanofibers, Lavanya et al. [232] used electrospinning and easy chemical methods. The interface between rGO and TiO_2 nanofibers in these composites favored an efficient photogenerated charge carrier separation with an enhanced efficiency of photocatalytic MO degradation of 96% instead of only 43% of TiO_2 nanofibers. Wang et al. [233] applied a low-temperature solvothermal method using graphite oxide and $TiCl_3$ as precursors to prepare GTiO_2Ns nanocomposites. During this solvothermal

transformation, the synthesis of TiO_2 nanoparticles and G formation occurred. Compared to only TiO_2 nanoparticles, also in this case, the results revealed a greatly enhanced visible light photocatalytic MO degradation.

Athanasekou et al. [234] prepared rGO-TiO_2 composite membranes for incorporation into a water purification device for the application in the hybrid photocatalytic/ultrafiltration process. For this, GO sheets were decorated with TiO_2 nanoparticles and deposited into the pores of ultrafiltration mono-channel monoliths using the dip-coating technique and water filtration conducted in the dark, as well as UV and visible light irradiation. The obtained results, compared with that of standard nanofiltration, showed that the synergetic effects of GO on MO adsorption and photocatalytic degradation demonstrated that this material can be positively applied in nanofiltration technology.

Liu [235] prepared rGO-TiO_2 with the hydrothermal method by using GO and $Ti(OH)_4$ in ethanol/water. The results showed that rGO-TiO_2 presented a stratified structure composed of dispersed anatase TiO_2 on the surface of rGO; the larger surface area of the composite was favorable for the MO absorption; in addition, the extension of the visible light region absorption range was observed. All these factors positively favored the photocatalytic performances of the composites in the photodegradation of MO under visible light irradiation with respect to that of pure TiO_2.

In Table 5, the different preparation methods of GTiO_2Ns applied in MO photodegradation are summarized.

Table 5. Photocatalytic applications of Graphene Based TiO_2 nanocomposites in the degradation of Methyl Orange.

Photoactive Nanomaterials	Dye Conc. (mg/L)	Catalyst Quantity (g/L)	Light Source	Irradiation Time (min)	Degradation (%)	Refs.
rGO/TiO_2 (mix anatase/ rutile nanofibers)	10	0.4	UV	120	97	[225]
G-pasted TiO_2 spheres	12	0.5	UV	75	95	[63]
GO/TiO_2	13	1 1	UV Vis	60 60	88 80	[226]
rGO/TiO_2		1 1	UV Vis	60 60	70 99	
rGO/TiO_2 anotube	20	0.25	UV	210	100	[227]
rGO/TiO_2	10	0.5	UV	75	70	[228]
rGO/TiO_2 mix anatasio/rutilio	6.55	0.6	UV Vis	100 100	100 50	[229]
G/TiO_2/Magnetite	9.6	0.16	UV	90	99	[230]
Flocculent likeTiO_2/G	20	0.8	UV	60	70	[231]
rGO/TiO_2 nanofibers	15	0.4	UV	120	100	[232]
G/TiO_2	10	0.6	UV	60	80	[233]
TiO_2/rGO	10	0.5	Vis	240	90	[235]

In addition, other authors explored photocatalytic materials in the photodegradation of *Rhodamine-B* (RB), which is a brilliant soluble basic dye, most used in the dyeing of various products of the textile industry such as cotton, silk, paper, leather, and others. Notably, RB imparts an intense color to polluted wastewaters derived from different industries and from scientific laboratories [236]. In particular, for RhB photodegradation, Chen Q. et al. [237] used electrospinning and the hydrothermal reaction in mixed ethanol/water solution to prepare nanocomposites composed from rGO and TiO_2 nanotubes. In these nanocomposites, TiO_2 nanotubes combined with rGO sheets between Ti-C and Ti-O-C bonds and the absorption edge shifted to higher wavelengths, improving the visible light absorption with respect to pure TiO_2 nanotubes. The measurements of photocatalytic activities

regarding RhB photodegradation under xenon lamp irradiation showed that the highest photocatalytic activities were obtained when the rGO ratio increased to 10%.

Furthermore, Chen Y. et al. [238] used a hydrothermal method to prepare rGO and TiO_2 hybrid of 10–20 nm, by using TiO_2 P25 nanoparticles and "liquid-exfoliated" GO. Also in this case, rGO-TiO_2, compared to only TiO_2, showed an increased photocatalytic RhB degradation under Xe lamp irradiation. The rGO-TiO_2 characterization confirmed the enhancement of photocatalytic and could be attributed to two reasons. The first was that rGO extended the path and lifetime of photogenerated electrons of TiO_2, minimizing the recombination of electron–hole pairs. while the second was that rG expanded the light absorption spectrum versus the visible light range. These effects were explained by the change of the energy gap and the likelihood of the up-conversion photoluminescence mechanism.

Another example was reported by Wang et al. [239] about the immobilization of anatase TiO_2 nanosheets on the magnetically actuated artificial cilia film by using rGO as the contact medium. The artificial cilia film was optimal in the immobilization of more powder of photocatalysts and, when used under s rotating magnetic field, exhibited an improvement of RhB degradation efficiency due to high mass transfer and to the efficiencies of photoproducts desorption. Biris et al. [240] synthesized core-shell nanostructural materials with multi-component architectures from TiO_2 and layers of graphitic materials by application CVD for 5, 10, 30, and 45 min with methane as the carbon source. The reaction time linearly regulated the quantity of G shells covering the TiO_2 surfaces, obtaining nanostructured materials with excellent stability and photocatalytic activity in the UV RhB degradation.

Moreover, Kim et al. [241] used synthesized composites of flower-like TiO_2 spheres and rGO (FTS-G). First TiO_2 spheres, with high specific surface area and good pore structure, and rGO without the use of strong reducing agents, were separately prepared; next, FTS-G were synthesized by using a solvothermal method. The photocatalytic performance of FTS-G was evaluated for RhB photodegradation under solar light irradiation, establishing that the rGO quantity was very important for the effects on photocatalytic activity. This preparation method could also be used to prepare other photocatalysts composed of flower-like TiO_2 spheres with carbon materials. Liu et al. [242] prepared a photocatalyst based on TiO_2 nanotubes and rGO with the hydrothermal method that was successively tested in the photocatalytic degradation of RhB under UV-light irradiation. Also with this photocatalyst, thanks to the introduction of rGO on TiO_2 nanotubes, the adsorption capacity as well as the photocatalytic activity in RhB photodegradation increased compared to the same without rGO.

Sedghi et al. [243], by using Titanium(IV) chloride as a photocatalyst precursor, prepared different nanocomposites of porous and magnetic porous GO in the mix with TiO_2 (anatase) and TiO_2 (mix phase), respectively. Between these nanocomposites, the mix of TiO_2 with magnetic porous GO showed enhanced efficiency in the RhB degradation under visible light irradiation compared with that of the other photocatalysts, obtaining 100% degradation in less than 20 min. Similarly, Zhang et al. [244] used the one-pot hydrothermal process, by using tetrabutyl titanate and GO, to prepare a series of self-assembled composites of anatase TiO_2 nanocrystals and three-dimensional graphene aerogel. The obtained composites showed higher adsorption capacities and good visible light efficiency in the RhB photodegradation. The results of this study clarified that the chemical-physical properties of these composites could be attributed to their 3D nanoporous structure with high surface areas and to the contemporary action of G nanosheets and TiO_2 nanoparticles.

An ultrasonication-assisted reduction process was used from He et al. [245] to produce rGO-TiO_2 nanocomposites. In this process, simultaneous GO reduction and TiO_2 crystals formation were obtained; photocatalytic studies demonstrated that the quantities rGO in these nanocomposites influenced the RhB degradation efficiency under visible light irradiation. The obtained increase in the photocatalytic activity was attributed in this case to the harvesting under visible-light irradiation and to the efficiency in the separation of the photogenerated charge carriers, also obtaining an improvement in the photoelectric conversion efficiency.

Fang et al. [246] exfoliated GO sheets from graphite and wrapped on the surfaces of polymer microspheres of about 2.5 μm in diameter. Successively, the solvothermal method permitted the nucleation and growth of anatase TiO_2 nanoparticles on the GO surfaces and the contemporary GO reduction to rGO. The as-prepared GO-skined GO/polymer hybrid microspheres composites tested in the photocatalytic activity with RhB solutions gave 96% degradation in 30 min under visible light irradiation, demonstrating an improvement with respect to commercial TiO_2. The results were attributed to the favorable interactions between rGO of singular electrical conductivity and TiO_2 nanoparticles.

Liang et al. [247] used a one-step hydrothermal approach to synthesize chemically bonded TiO_2/rGO nanocomposites by using $Ti(SO_4)_2$ and GO as precursors and ethanol/water solvent as a reducing agent, obtaining well-dispersed TiO_2 nanocrystals on the surface of rGO sheets with optimal interfacial contact. The obtained nanocomposites demonstrated higher photocatalytic activity with respect to only TiO_2 nanoparticles and to a simple mixing of TiO_2 and rGO samples in the RhB degradation which was attributed, also in this case, to the interaction between TiO_2 and rGO, with excellent electron trapping and transportation properties.

Li et al. [248] obtained different carbon materials-TiO_2 hybrid nanostructures incorporated into TiO_2, activated carbon, G, carbon nanotubes, and fullerene by using a solvothermal method and thermal annealing. The relationships between the interactions of carbon materials with TiO_2 nanoparticles, morphologies, structures, and increasing photodegradation performances in RhB degradation were clarified. The results of these photocatalysts were due to higher adsorption properties, the favorable formation of chemical bonds of Ti-O-C, reduced band gap, lower particle size, and charge-carrier qualities. In Table 6, the different preparation methods of GTiO_2Ns applied in RhB photodegradation are listed.

Table 6. Photocatalytic applications of Graphene Based TiO_2 nanocomposites in the degradation of Rhodamin B.

Photoactive Nanomaterials	Dye Conc. (mg/L)	Catalyst Quantity (g/L)	Light Source	Irradiation Time (min)	Degradation (%)	Refs.
TiO_2/rGO	30	0.2	Vis	40	100	[238]
rGO/TiO_2 nanosheets onmagnetically cilia film rGO/TiO_2-Au	20	0.2	UV	180	83 100	[239]
Core-shell TiO_2/G	4.79	0.6	UV	270	100	[240]
Flower-like TiO_2 sphere /rGO	15	0.4	Simulated solar	120	100	[241]
TiO_2 nanotubes/rGO	10	0.5	UV	20	100	[242]
TiO_2/magnetic porous GO	10	0. 1	Vis	20	100	[243]
3D TiO_2/G aerogel	20	0.2	Visible light	180	99	[244]
TiO_2/rGO	4.79	0.4	Visible light	180	100	[245]
TiO_2/rGO/polymer	8	0.2	Visible light	30	96	[246]
TiO_2/rGO	20	0.5	UV	30	100	[247]
GTiO_2	5	0.5	Visible light	60	80	[248]

Rhodamine 6G (Rh6G) is dark reddish-purple dye, mostly used in the textile industries, in biochemistry research laboratories, and in other applications. Rh6G is a non-volatile compound that presents high solubility in water causing skin, eye, and respiratory system irritations, and is also carcinogenic and poisonous to living organisms [249].

In order to obtain the photocatalytic degradation of Rh6G, Pu et al. [194] demonstrated a facile and environmentally friendly strategy for the simultaneous in situ preparation of the rGO-TiO_2 "dyade hybrid" obtained by the photoreduction of GO nanosheets in ethanolic solutions of GO and TiO_2 (P25) mix. Successively, the photodegradation efficiency of the resultant composite by utilizing

Rh6G as the target pollutant was systematically investigated. The obtained rGO-TiO_2 presented a significant enhancement in photo energy adsorption, leading to the effective photocatalytic degradation reactions which exhibited more than triple the higher photodegradation rate compared to commercial TiO_2 (P25) nanoparticles.

Reactive Black 5 (RB5), which has two azo groups, belongs to the class of azo reactive dyes, which are abundantly used in textile industries for dyeing.

The photocatalytic degradation of RB5 was studied by Day et al. [250], who prepared different types of GTiO_2Ns nanocomposites with G and P25 or Titanium (IV) n-butoxide as precursors by using the hydrothermal method. To investigate the differences of the photocatalytic properties of composites with various TiO_2 shapes, nanotubes, nanosheets, and nanoparticles of TiO_2 were prepared and combined with G. The photocatalytic activities of these composites were tested in the degradation of RB5 under UV lamp irradiation, indicating that the differences in the TiO_2 morphology and the characteristics of heterojunction between G and TiO_2 played an important role in the photocatalytic abilities. The results demonstrated that these composites exhibited excellent adsorption capacity and higher photocatalytic activity with respect to P25, and that the photocatalytic activity of GTiO_2Ns nanosheets was higher than those of the other tested photocatalysts. Another example was proposed by Liang et al. [251], who obtained an increase of photocatalysis efficiency for RB5 by using TiO_2 nanotubes and G nanocomposites prepared with the hydrothermal method. In particular, Zhang et al. [252] deciphered the mechanism of RB5 photodegradation, which was used as a model for other azo dyes by using G-loaded TiO_2 as a photocatalyst. They demonstrated that electronic transfer groups affect the degradability of azo dyes, that $^{\bullet}$OH radicals are the major oxidized species, and that substituents with high electron-density in the dye structure were more favorably attacked by $^{\bullet}$OH radicals.

The photodegradation of the non-biodegradable azo dye *acid orange 7* (AO7) in aqueous solution was studied by Posa et al. [253] who, by using GTiO_2Ns nanocomposites, obtained an improvement of photocatalytic performance compared with that of pure TiO_2, examining also the reusability of the photocatalyst. They suggested a reaction mechanism on the basis of the obtained results. Furthermore, Gao et al. [254] synthesized different TiO_2 nanostructures: one-dimensional TiO_2 nanotubes and nanowires, three-dimensional spheres assembled by nanoparticles and by nanosheets. The results of photodegradation activity in the AO7 degradation indicated that the photodegradation efficiency of TiO_2 spheres assembled by nanosheets was the highest with respect to the other TiO_2 nanostructures, while its specific surface area was lower than that of TiO_2 nanotubes. The results were attributed to the highest light harvesting capacity under solar light derived from the multiple reflections of light, and from the hierarchical mesoporous structure. The last example regards the study of Muthirulan et al. [255], who fabricated GTiO_2Ns by using a simple one-step chemical process, mixing TiO_2 nanoparticles suspended in ethanol with G followed by ultrasonication and successive treatment in a rotary evaporator under vacuum. The dried GTiO_2Ns showed improvement in the photocatalytic ability in the degradation of AO7 under both UV and solar light irradiations. The obtained results of photodegradation indicated that GTiO_2Ns nanocomposites exhibited higher photocatalytic activity than that of TiO_2, which was attributed to the role of G in the suppression of charge recombination and in the promotion of the charge transfer, permitting also a possible reaction pathway for the degradation of AO7.

6. Conclusions

In this short review, we have described the characteristics of both TiO_2 semiconductors and graphene materials and reported several examples focusing on the recent progress in the design, synthesis, and applications of these GTiO_2Ns nanocomposites used as photocatalysts in the photocatalytic degradation of synthetic dyes.

We have described the important effects of G in GTiO_2Ns nanocomposites, as shown in Figure 6. In fact, in conjunction with TiO_2 nanomaterials, G can act as a co-adsorbent thanks to the increase of adsorption surface and to π-π interactions with dye and as a sensitizer due to the electron transfer from

the G photoexcited state, with delocalization and energy excess dissipation, to the TiO_2 surface with the extension of the light absorption towards the visible region. Notably, both the functions of conductive materials and co-catalysts favor the stabilization of excited electrons, thus limiting the electron-hole recombination in the photocatalytic process. In addition to these properties, TiO_2 band-gap narrowing due to the interaction between TiO_2 and G was demonstrated.

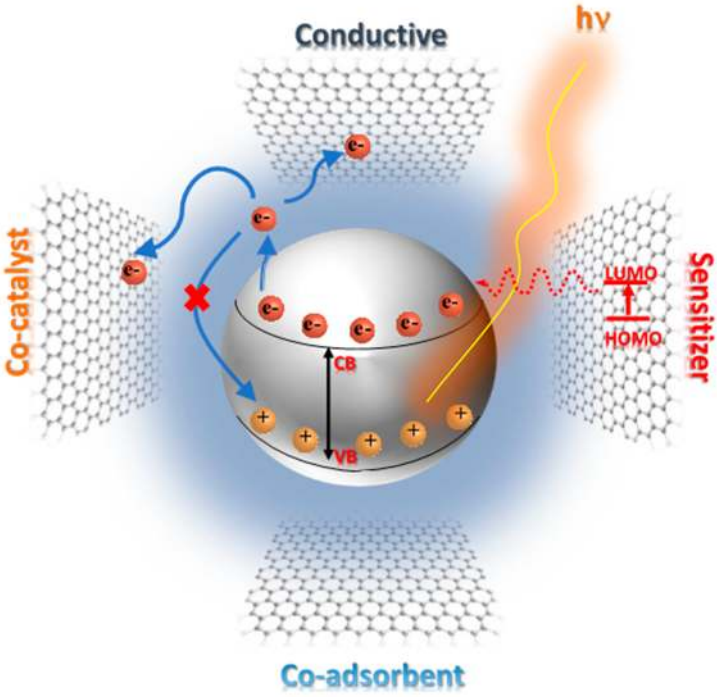

Figure 6. Schematic representation of the main features of graphene in the photocatalysis with TiO_2.

Thanks to these features, in order to obtain the best benefit of graphene in the enhancment of the photoactivity of TiO_2 nanomaterials, all of these factors that dominate the photocatalytic process must to be taken into consideration and optimized with the purpose of obtaining the best dye absorption and its complete mineralization.

Much research has been conducted regarding the photocatalytic degradation of synthetic dyes, and the high-quality results of these studies demonstrate that these materials could be promising for large-scale applications in wastewater depuration.

Acknowledgments: This work was partially supported from FAR Project NAMES: "Nanocomposite Materials for Energy and Environment Applications" of Camerino University.

Author Contributions: Rita Giovannetti organized and prepared the manuscript. Elena Rommozzi collected and analyzed the literature reports, Marco Zannotti, Chiara Anna D'Amato designed the figures and critically revised the manuscript.

Conflicts of Interest: The authors declare no conflict of interest.

References

1. Peirce, J.J.; Weiner, R.; Vesilind, P.A. *Environmental Pollution and Control*, 4th ed.; Elsevier: Oxford, UK, 1998; ISBN 978-0-7506-9899-3.
2. Andreozzi, R.; Caprio, V.; Insola, A.; Marotta, R. Advanced oxidation processes (AOP) for water purification and recovery. *Catal. Today* **1999**, *53*, 51–59. [CrossRef]
3. Chaukura, N.; Edna, C.; Murimba, E.C.; Gwenzi, W. Sorptive removal of methylene blue from simulated wastewater using biochars derived from pulp and paper sludge. *Environ. Technol. Innov.* **2017**, *8*, 132–140. [CrossRef]

4. Solís, M.; Solís, A.; Inés Pérez, H.; Manjarrez, N.; Flores, M. Microbial decolouration of azo dyes: A review. *Process. Biochem.* **2012**, *47*, 1723–1748. [CrossRef]
5. Zhang, Z.; Yang, R.Y.; Gao, Y.S.; Zhao, Y.F.; Wang, J.Y.; Huang, L.; Guo, J.; Zhou, T.T.; Lu, P.; Guo, Z.H.; et al. Novel $Na_2Mo_4O_{13}/\alpha$-MoO_3 hybrid material as highly efficient CWAO catalyst for dye degradation at ambient conditions. *Sci. Rep.* **2014**, *4*, 6797–6809. [CrossRef] [PubMed]
6. Santhosh, C.; Velmurugan, V.; Jacob, G.; Jeong, S.K.; Grace, A.N.; Bhatnagar, A. Role of nanomaterials in water treatment applications: A review. *Chem. Eng. J.* **2016**, *306*, 1116–1137. [CrossRef]
7. Padikkaparambil, S.; Narayanan, B.; Yaakob, Z.; Viswanathan, S.; Tasirin, S.M. Au/TiO_2 reusable photocatalysts for dye degradation. *Int. J. Photoenergy* **2013**, *2013*. [CrossRef]
8. Cho, K.M.; Kim, K.H.; Choi, H.O.; Jung, H.T. A highly photoactive, visible-light-driven graphene/2D mesoporous TiO_2 photocatalyst. *Green Chem.* **2015**, *17*, 3972–3978. [CrossRef]
9. Ibhadon, A.O.; Fitzpatrick, P. Heterogeneous photocatalysis: Recent advances and applications. *Catalysts* **2013**, *3*, 189–218. [CrossRef]
10. Wei, W.; Liu, D.; Wei, Z.; Zhu, Y. Short-range π-π stacking assembly on P25 TiO_2 nanoparticle for enhanced visible-light photocatalysis. *ACS Catal.* **2017**, *7*, 652–663. [CrossRef]
11. Jiang, W.J.; Liu, Y.F.; Wang, J.; Zhang, M.; Luo, W.J.; Zhu, Y.F. Separation-free polyaniline/TiO_2 3D hydrogel with high photocatalytic activity. *Adv. Mater. Interfaces* **2016**, *3*, 9.
12. Tatsuma, T.; Saitoh, S.; Ohko, Y.; Fujishima, A. TiO_2-WO_3 photoelectrochemical anticorrosion system with an energy storage ability. *Chem. Mater.* **2001**, *13*, 2838–2842. [CrossRef]
13. Sajan, C.P.; Wageh, S.; Al-Ghamdi, A.A.; Yu, J.G.; Cao, S.W. TiO_2 nanosheets with exposed {001} facets for photocatalytic applications. *Nano Res.* **2016**, *9*, 3–27. [CrossRef]
14. Chen, X.; Mao, S.S. Titanium dioxide nanomaterials: Synthesis, properties, modifications, and applications. *Chem. Rev.* **2007**, *107*, 2891–2959. [CrossRef] [PubMed]
15. Tong, H.; Ouyang, S.X.; Bi, Y.P.; Umezawa, N.; Oshikiri, M.; Ye, J.H. Nano-photocatalytic materials: Possibilities and challenges. *Adv. Mater.* **2012**, *24*, 229–251. [CrossRef] [PubMed]
16. Anpo, M.; Tackeuchi, M. The design and development of highly reactive titanium oxide photocatalysts operating under visible light irradiation. *J. Catal.* **2003**, *216*, 505–516. [CrossRef]
17. Al-Harbi, L.M.; El-Mossalamy, E.H.; Arafa, H.M.; Al-Owais, A.; Shah, M.A. TiO_2 Nanoparticles with Tetra-pad Shape Prepared by an Economical and Safe Route at very Low Temperature. *Mod. Appl. Sci.* **2011**, *5*, 130–135. [CrossRef]
18. Giovannetti, R.; D'Amato, C.A.; Zannotti, M.; Rommozzi, E.; Gunnella, R.; Minicucci, M.; Di Cicco, A. Visible light photoactivity of polypropylene coated nano-TiO_2 for dyes degradation in water. *Sci. Rep.* **2015**, *2*. [CrossRef] [PubMed]
19. Augugliaro, V.; Bellardita, M.; Loddo, V.; Palmisano, G.; Palmisano, L.; Yurdakal, S. Overview on oxidation mechanisms of organic compounds by TiO_2 in heterogeneous photocatalysis. *J. Photochem. Photobiol. C Photochem. Rev.* **2012**, *13*, 224–245. [CrossRef]
20. Sud, D.; Kaur, P. Heterogeneous photocatalytic degradation of selected organophosphate pesticides: A review. *Crit. Rev. Environ. Sci. Technol.* **2012**, *42*, 2365–2407. [CrossRef]
21. Wang, J.L.; Xu, L.J. Advanced oxidation processes for wastewater treatment: Formation of hydroxyl radical and application. *Crit. Rev. Environ. Sci. Technol.* **2012**, *42*, 251–325. [CrossRef]
22. Hashimoto, K.; Irie, H.; Fujishima, A. TiO_2 photocatalysis: A historical overview and future prospects. *Jpn. J. Appl. Phys.* **2005**, *12*, 8269–8285. [CrossRef]
23. Sheikh, M.U.D.; Naikoo, G.A.; Thomas, M.; Bano, M.; Khan, F. Solar-assisted photocatalytic reduction of methyl orange azo dye over porous TiO_2 nanostructures. *New J. Chem.* **2016**, *40*, 5483–5494. [CrossRef]
24. Zhang, N.; Zhang, Y.; Xu, Y.-J. Recent progress on graphene-based photocatalysts: Current status and future perspectives. *Nanoscale* **2012**, *4*, 5792–5813. [CrossRef] [PubMed]
25. Malato, S.; Fernández-Ibáñez, P.; Maldonado, M.I.; Blanco, J.; Gernjak, W. Decontamination and disinfection of water by solar photocatalysis: Recent overview and trends. *Catal. Today* **2009**, *147*, 1–59. [CrossRef]
26. Wang, W.K.; Chen, J.J.; Gao, M.; Huang, Y.X.; Zhang, X.; Yu, H.Q. Photocatalytic degradation of atrazine by boron-doped TiO_2 with a tunable rutile/anatase ratio. *Appl. Catal. B Environ.* **2016**, *195*, 69–76. [CrossRef]
27. Hao, R.R.; Wang, G.H.; Tang, H.; Sun, L.L.; Xu, C.; Han, D.Y. Template-free preparation of macro/mesoporous g-C_3N_4/TiO_2 heterojunction photocatalysts with enhanced visible light photocatalytic activity. *Appl. Catal. B Environ.* **2016**, *187*, 47–58. [CrossRef]

28. Gua, Y.; Xinga, M.; Zhang, J. Synthesis and photocatalytic activity of graphene based doped TiO_2 nanocomposites. *Appl. Surf. Sci.* **2014**, *319*, 8–15. [CrossRef]
29. Zaleska, A. Doped-TiO_2: A review. *Recent Pat. Eng.* **2008**, *2*, 157–164. [CrossRef]
30. Yang, H.G.; Sun, C.H.; Qiao, S.Z.; Zou, J.; Liu, G.; Smith, S.C.; Cheng, H.M.; Lu, G.Q. Anatase TiO_2 single crystals with a large percentage of reactive facets. *Nature* **2008**, *453*, 638–641. [CrossRef] [PubMed]
31. Adán, C.; Bahamonde, A.; Fernández-García, M.; Martínez-Arias, A. Structure and activity of nanosized iron-doped anatase TiO_2 catalysts for phenol photocatalytic degradation. *Appl. Catal. B Environ.* **2007**, *72*, 11–17. [CrossRef]
32. Cai, J.; Wu, X.; Li, S.; Zheng, F. Controllable location of Au nanoparticles as cocatalyst onto TiO_2@CeO_2 nanocomposite hollow spheres for enhancing photocatalytic activity. *Appl. Catal. B Environ.* **2017**, *201*, 12–21. [CrossRef]
33. Cheng, L.; Qiu, S.; Chen, J.; Shao, J.; Cao, S. A practical pathway for the preparation of Fe_2O_3 decorated TiO_2 photocatalyst with enhanced visible-light photoactivity. *Mater. Chem. Phys.* **2017**, *190*, 53–61. [CrossRef]
34. Xie, Y.; Meng, Y.; Wu, M. Visible-light-driven self-cleaning SERS substrate of silver nanoparticles and graphene oxide decorated nitrogen-doped Titania nanotube array. *Surf. Interface Anal.* **2016**, *48*, 334–340. [CrossRef]
35. Xing, Z.; Zong, X.; Zhu, Y.; Chen, Z.; Bai, Y.; Wang, L. A nanohybrid of CdTe@CdS nanocrystals and Titania nanosheets with p-n nanojunctions for improved visible light-driven hydrogen production. *Catal. Today* **2016**, *264*, 229–235. [CrossRef]
36. Hamzezadeh-Nakhjavani, S.; Tavakoli, O.; Akhlaghi, S.P.; Salehi, Z.; Esmailnejad-Ahranjani, P.; Arpanaei, A. Efficient photocatalytic degradation of organic pollutants by magnetically recoverable nitrogen-doped TiO_2 nanocomposite photocatalysts under visible light irradiation. *Environ. Sci. Pollut. Res.* **2015**, *22*, 18859–18873. [CrossRef] [PubMed]
37. Qi, K.; Selvaraj, R.; Al Fahdi, T.; Al-Kindy, S.; Kim, Y.; Wang, G.-C.; Tai, C.-W.; Sillanpää, M. Enhanced photocatalytic activity of anatase-TiO_2 nanoparticles by fullerene modification: A theoretical and experimental study. *Appl. Surf. Sci.* **2016**, *387*, 750–758. [CrossRef]
38. Qin, X.; He, F.; Chen, L.; Meng, Y.; Liu, J.; Zhao, N.; Huang, Y. Oxygen-vacancy modified TiO_2 nanoparticles as enhanced visible-light driven photocatalysts by wrapping and chemically bonding with graphite-like carbon. *RSC Adv.* **2016**, *6*, 10887–10894. [CrossRef]
39. Rahbar, M.; Behpour, M. Multi-walled carbon nanotubes/TiO_2 thin layer for photocatalytic degradation of organic pollutant under visible light irradiation. *J. Mater. Sci. Mater. Electron.* **2016**, *27*, 8348–8355. [CrossRef]
40. Lin, L.; Wang, H.; Xu, P. Immobilized TiO_2-reduced graphene oxide nanocomposites on optical fibers as high performance photocatalysts for degradation of pharmaceuticals. *Chem. Eng. J.* **2017**, *310*, 389–398. [CrossRef]
41. Stoller, M.D.; Park, S.; Zhu, Y.; An, J.; Ruoff, R.S. Graphene-based ultracapacitors. *Nano Lett.* **2008**, *8*, 3498–3502. [CrossRef] [PubMed]
42. Novoselov, K.S.; Geim, A.K.; Morozov, S.V.; Jiang, D.; Zhang, Y.; Dubonos, S.V.; Grigorieva, I.V.; Firsov, A.A. Electric field effect in atomically thin carbon films. *Science* **2004**, *306*, 666–669. [CrossRef] [PubMed]
43. Balandin, A.A.; Ghosh, S.; Bao, W.; Calizo, I.; Teweldebrhan, D.; Miao, F.; Lau, C.N. Superior thermal conductivity of single-layer graphene. *Nano Lett.* **2008**, *8*, 902–907. [CrossRef] [PubMed]
44. Cheng, Y.; Zhou, S.; Hu, P.; Zhao, G.; Li, Y.; Zhang, X.; Han, W. Enhanced mechanical, thermal, and electric properties of graphene aerogels via supercritical ethanol drying and high-temperature thermal reduction. *Sci. Rep.* **2017**, *7*. [CrossRef] [PubMed]
45. Sun, W.; Du, A.; Gao, G.; Shen, J.; Wu, G. Graphene-templated carbon aerogels combining with ultra-high electrical conductivity and ultra-low thermal conductivity. *Microporous Mesoporous Mater.* **2017**, *253*, 71–79. [CrossRef]
46. Tran, V.-T.; Saint-Martin, J.; Dollfus, P.; Volz, S. Optimizing the thermoelectric performance of graphene nano-ribbons without degrading the electronic properties. *Sci. Rep.* **2017**, *7*. [CrossRef] [PubMed]
47. Wei, A.; Li, Y.; Li, Y.; Ye, H. Thermal characteristics of graphene nanosheet with graphane domains of varying morphologies. *Comput. Mater. Sci.* **2017**, *138*, 192–198. [CrossRef]
48. Geim, A.K.; Novoselov, K.S. The rise of graphene. *Nat. Mater.* **2007**, *6*, 183–191. [CrossRef] [PubMed]
49. Leary, R.; Westwood, A. Carbonaceous nanomaterials for the enhancement of TiO_2 photocatalysis. *Carbon* **2011**, *49*, 741–772. [CrossRef]

50. Hamandia, M.; Berhault, G.; Guillardb, C.; Kochkara, H. Influence of reduced graphene oxide on the synergism between rutileand anatase TiO_2 particles in photocatalytic degradation of formic acid. *Mol. Catal.* **2017**, *432*, 125–130. [CrossRef]
51. Morales-Torres, S.; Pastrana-Martínez, L.M.; Figueiredo, J.L.; Faria, J.J.; Silva, A.M.T. Design of graphene-based TiO_2 photocatalysts—A review. *Environ. Sci. Pollut. Res.* **2012**, *19*, 3676–3687. [CrossRef] [PubMed]
52. Adamu, H.; Dubey, P.; Anderson, J.A. Probing the role of thermally reduced graphene oxide in enhancing performance of TiO_2 in photocatalytic phenol removal from aqueous environments. *Chem. Eng. J.* **2016**, *284*, 380–388. [CrossRef]
53. Giovannetti, R.; Rommozzi, E.; Zannotti, M.; D'Amato, C.A.; Ferraro, S.; Cespi, M.; Bonacucina, G.; Minicucci, M.; Di Cicco, A. Exfoliation of graphite into graphene in aqueous solution: An application as graphene/TiO_2 nanocomposite to improve visible light photocatalytic activity. *RSC Adv.* **2016**, *6*, 93048–93055. [CrossRef]
54. Truppi, A.; Petronella, F.; Placido, T.; Striccoli, M.; Agostiano, A.; Curri, M.L.; Comparelli, R. Visible-light-active TiO_2-based hybrid nanocatalysts for environmental applications. *Catalysts* **2017**, *7*, 100. [CrossRef]
55. Xiang, Q.; Yu, J.; Jaroniec, M. Graphene-based semiconductor photocatalysts. *Chem. Soc. Rev.* **2012**, *41*, 782–796. [CrossRef] [PubMed]
56. Zhang, Y.; Tang, Z.R.; Fu, X.Y.; Xu, J. TiO_2-graphene nanocomposites for gas-phase photocatalytic degradation of volatile aromatic pollutant: Is TiO_2-graphene truly different from other TiO_2-carbon composite materials? *ACS Nano* **2010**, *4*, 7303–7314. [CrossRef] [PubMed]
57. Surender Kumar, S. *Complex Magnetic Nanostructures: Synthesis, Assembly and Applications*; Springer: Cham, Switzerland, 2017.
58. Syväjärvi, M.; Tiwari, A. *Graphene Materials: Fundamentals and Emerging Applications*; Wiley: Hoboken, NJ, USA, 2015.
59. Singh, V.; Joung, D.; Zhai, L.; Das, S.; Khondaker, S.I.; Seal, S. Graphene based materials: Past, present and future. *Progress Mater. Sci.* **2011**, *56*, 1178–1271. [CrossRef]
60. Cong, H.-P.; Chena, J.-F.; Yu, S.-H. Graphene-based macroscopic assemblies and architectures: An emerging material system. *Chem. Soc. Rev.* **2014**, *43*, 7295–7325. [CrossRef] [PubMed]
61. Mahmood, N.; Zhang, C.; Yin, H.; Hou, Y. Graphene-based nanocomposites for energy storage and conversion in lithium batteries, supercapacitors and fuel cells. *J. Mater. Chem. A* **2014**, *2*, 15–32. [CrossRef]
62. Li, X.; Yu, J.; Wageh, S.; Al-Ghamdi, A.A.; Xie, J. Graphene in photocatalysis: A review. *Small* **2016**, *12*, 6640–6696. [CrossRef] [PubMed]
63. Xu, C.; Zhu, J.; Yuan, R.; Fu, X. More effective use of graphene in photocatalysis by conformal attachment of small sheets to TiO_2 spheres. *Carbon* **2016**, *96*, 394–402. [CrossRef]
64. Zhu, J.; Yang, D.; Yin, Z.; Yan, Q.; Zhang, H. Graphene and graphene-based materials for energy storage applications. *Small* **2014**, *10*, 3480–3498. [CrossRef] [PubMed]
65. Piao, Y. Preparation of porous graphene-based nanomaterials for electrochemical energy storage devices. In *Nano Devices and Circuit Techniques for Low-Energy Applications and Energy Harvesting*; Kyung, C.M., Ed.; KAIST Research Series; Springer: Dordrecht, The Netherland, 2016.
66. Li, N.; Liu, G.; Zhen, C.; Li, F.; Zhang, L.; Cheng, H.M. Battery performance and photocatalytic activity of mesoporous anatase TiO_2 nanospheres/graphene composites by template-free self-assembly. *Adv. Funct. Mater.* **2011**, *21*, 1717–1722. [CrossRef]
67. Maroni, F.; Raccichini, R.; Birrozzi, A.; Carbonari, G.; Tossici, R.; Croce, F.; Marassi, R.; Nobili, F. Graphene/silicon nanocomposite anode with enhanced electrochemical stability for lithium-ion battery applications. *J. Power Sources* **2014**, *269*, 873–882. [CrossRef]
68. Kaplas, T.; Kuzhir, P. Ultra-thin Graphitic Film: Synthesis and Physical Properties. *Nanoscale Res. Lett.* **2016**, *11*, 54. [CrossRef] [PubMed]
69. Allagui, A.; Abdelkareem, M.A.; Alawadhi, H.; Elwakil, A.S. Reduced graphene oxide thin film on conductive substrates by bipolar electrochemistry. *Sci. Rep.* **2016**, *6*. [CrossRef] [PubMed]
70. Bhuyan, M.S.A.; Uddin, M.N.; Islam, M.M.; Bipasha, F.A.; Hossain, S.S. Synthesis of graphene. *Int. Nano Lett.* **2016**, *6*, 65–83. [CrossRef]

71. Tetlow, H.; de Boer, J.P.; Ford, I.J.; Vvedenskyb, D.D.; Coraux, J.; Kantorovich, L. Growth of epitaxial graphene: Theory and experiment. *Phys. Rep.* **2014**, *542*, 195–295. [CrossRef]
72. Cui, Y.; Zhang, H.; Chen, W.; Yang, Z.; Cai, Q. Structural evolution of flower defects and effects on the electronic structures of epitaxial graphene. *J. Phys. Chem. C* **2017**, *121*, 15282–15287. [CrossRef]
73. Galves, L.A.; Wofford, J.M.; Soares, G.V.; Jahn, U.; Pfüller, C.; Riechert, H.; Lopes, J.M.J. The effect of the SiC(0001) surface morphology on the growth of epitaxial mono-layer graphene nanoribbons. *Carbon* **2017**, *115*, 162–168. [CrossRef]
74. Ramnani, P.; Neupane, M.R.; Ge, S.; Balandin, A.A.; Lake, R.K.; Mulchandani, A. Raman spectra of twisted CVD bilayer graphene. *Carbon* **2017**, *123*, 302–306. [CrossRef]
75. Chena, X.; Zhangb, L.; Chena, S. Large area CVD growth of graphene. *Synth. Met.* **2015**, *210*, 95–108. [CrossRef]
76. Zhang, Y.; Zhang, L.; Zhou, C. Review of chemical vapor deposition of graphene and related applications. *Acc. Chem. Res.* **2013**, *46*, 2329–2339. [CrossRef] [PubMed]
77. Lukosius, M.; Dabrowski, J.; Kitzmann, J.; Fursenko, O.; Akhtar, F.; Lisker, M.; Lippert, G.; Schulze, S.; Yamamoto, Y.; Schubert, M.A.; et al. Metal-free CVD graphene synthesis on 200 mm Ge/Si(001) substrates. *ACS Appl. Mater. Interfaces* **2016**, *8*, 33786–33793. [CrossRef] [PubMed]
78. Robert, M.; Jacobberger, R.M.; Machhi, R.; Wroblewski, J.; Ben Taylor, B.; Anne Lynn Gillian-Daniel, A.L.; Arnold, M.S. Simple graphene synthesis via chemical vapor deposition. *J. Chem. Educ.* **2015**, *92*, 1903–1907.
79. Kim, K.S.; Zhao, Y.; Jang, H.; Lee, S.Y.; Kim, J.M.; Kim, K.S.; Ahn, J.H.; Kim, P.; Choi, J.Y.; Hong, B.H. Large-scale pattern growth of graphene films for stretchable transparent electrodes. *Nature* **2009**, *457*, 706–710. [CrossRef] [PubMed]
80. Emtsev, K.V.; Bostwick, A.; Horn, K.; Jobst, J.; Kellogg, G.L.; Ley, L.; McChesney, J.L.; Ohta, T.; Reshanov, S.A.; Rohrl, J.; et al. Towards wafer-size graphene layers by atmospheric pressure graphitization of silicon carbide. *Nat. Mater.* **2009**, *8*, 203–207. [CrossRef] [PubMed]
81. Juang, Z.Y.; Wu, C.Y.; Lu, A.Y.; Su, C.Y.; Leou, K.C.; Chen, F.R.; Tsai, C.H. Graphene synthesis by chemical vapor deposition and transfer by a roll-to-roll process. *Carbon* **2010**, *48*, 3169–3174. [CrossRef]
82. Wei, D.C.; Liu, Y.Q.; Wang, Y.; Zhang, H.L.; Huang, L.P.; Yu, G. Synthesis of N-doped graphene by chemical vapor deposition and its electrical properties. *Nano Lett.* **2009**, *9*, 1752–1758. [CrossRef] [PubMed]
83. Zhang, H.; Zhang, X.; Sun, X.; Ma, Y. Shape-controlled synthesis of nanocarbons through direct conversion of carbon dioxide. *Sci. Rep.* **2013**, *3*. [CrossRef] [PubMed]
84. Hajian, M.; Zareie, M.; Hashemiana, D.; Bahrami, M. Synthesis of graphene through direct decomposition of CO_2. *RSC Adv.* **2016**, *6*, 73331–73335. [CrossRef]
85. Qin, B.; Zhang, T.; Chen, H.; Ma, Y. The growth mechanism of few-layer graphene in the arc discharge process. *Carbon* **2016**, *102*, 494–498. [CrossRef]
86. Poorali, M.S.; Bagheri-Mohagheghi, M.M. Synthesis and physical properties of multi-layered graphene sheets by Arc-discharge method with TiO_2 and ZnO catalytic. *J. Mater. Sci. Mater. Electron.* **2017**, *28*, 6186–6193. [CrossRef]
87. Xiao, B.; Li, X.; Li, X.; Wang, B.; Langford, C.; Li, R.; Sun, X. Graphene Nanoribbons Derived from the Unzipping of Carbon Nanotubes: Controlled Synthesis and Superior Lithium Storage. *J. Phys. Chem. C* **2014**, *118*, 881–890. [CrossRef]
88. Yang, X.; Dou, X.; Rouhanipour, A.; Zhi, L.; Räder, H.J.; Mülle, K. Two-dimensional graphene nanoribbons. *J. Am. Chem. Soc.* **2008**, *130*, 4216–4217. [CrossRef] [PubMed]
89. Kharisov, B.I.; Kharissova, O.V. Synthesis of graphene by pyrolysis of organic matter. In *Graphene Science Handbook: Fabrication Methods*; Aliofkhazraei, M., Ali, N., Milne, W.I., Ozkan, C.S., Mitura, S., Gervasoni, J.L., Eds.; CRC Press: Boca Raton, FL, USA, 2016; pp. 345–360.
90. Zou, B.; Wang, X.X.; Huang, X.X.; Wang, J.N. Continuous synthesis of graphene sheets by spray pyrolysis and their use as catalysts for fuel cells. *Chem. Commun.* **2015**, *51*, 741–744. [CrossRef] [PubMed]
91. Jabari-Seresht, R.; Jahanshahi, M.; Rashidi, A.; Ghoreyshi, A.A. Fabrication and evaluation of nonporous graphene by a unique spray pyrolysis method. *Chem. Eng. Technol.* **2013**, *36*, 1550–1558. [CrossRef]
92. Khan, M.; Tahir, M.N.; Adil, S.F.; Khan, H.U.; Siddiqui, M.R.H.; Al-warthan, A.A.; Tremel, W. Graphene based metal and metal oxide nanocomposites: Synthesis, properties and their applications. *J. Mater. Chem. A* **2015**, *3*, 18753–18808. [CrossRef]

93. Kim, H.; Abdala, A.A.; Macosko, C.W. Graphene/polymer nanocomposites. *Macromolecules* **2010**, *43*, 6515–6530. [CrossRef]
94. Yi, M.; Shen, Z. A review on mechanical exfoliation for the scalable production of graphene. *J. Mater. Chem. A* **2015**, *3*, 11700–11715. [CrossRef]
95. Hernandez, Y.; Nicolosi, V.; Lotya, M.; Blighe, F.M.; Sun, Z.Y.; De, S.; McGovern, I.T.; Holland, B.; Byrne, M.; Gunko, Y.K.; et al. High-yield production of graphene by liquid-phase exfoliation of graphite. *Nat. Nanotechnol.* **2008**, *3*, 563–568. [CrossRef] [PubMed]
96. Li, X.; Zhang, G.; Bai, X.; Sun, X.; Wang, X.; Wang, E.; Dai, H. Highly conducting graphene sheets and Langmuir-Blodgett films. *Nat. Nanotechnol.* **2008**, *3*, 538–542. [CrossRef] [PubMed]
97. Coscia, U.; Palomba, M.; Ambrosone, G.; Barucca, G.; Cabibbo, M.; Mengucci, P.; de Asmundis, R.; Carotenuto, G. A new micromechanical approach for the preparation of graphene nanoplatelets deposited on polyethylene. *Nanotechnology* **2017**, *28*. [CrossRef] [PubMed]
98. Zhong, Y.L.; Swager, T.M. Enhanced electrochemical expansion of graphite for in situ electrochemical functionalization. *J. Am. Chem. Soc.* **2012**, *134*, 17896–17899. [CrossRef] [PubMed]
99. Leroux, Y.R.; Jean-François Bergamini, J.-F.; Ababou, S.; Le Breton, J.-C.; Hapiot, P. Synthesis of functionalized few-layer graphene through fast electrochemical expansion of graphite. *J. Electroanal. Chem.* **2015**, *753*, 42–46. [CrossRef]
100. Hossaina, S.T.; Wanga, R. Electrochemical exfoliation of graphite: Effect of temperature and hydrogen peroxide addition. *Electrochim. Acta* **2016**, *216*, 253–260. [CrossRef]
101. McAllister, M.J.; Li, J.L.; Adamson, D.H.; Schniepp, H.C.; Abdala, A.A.; Liu, J.; Herrera-Alonso, M.; Milius, D.L.; Car, R.; Prudhomme, R.K.; et al. Single sheet functionalized graphene by oxidation and thermal expansion of graphite. *Chem. Mater.* **2007**, *19*, 4396–4404. [CrossRef]
102. Beidaghi, M.; Wang, Z.; Gu, L.; Wang, C. Electrostatic spray deposition of graphene nanoplatelets for high-power thin-film supercapacitor electrodes. *J. Solid State Electrochem.* **2012**, *16*, 3341–3348. [CrossRef]
103. Allen, M.J.; Tung, V.C.; Kaner, R.B. Honeycomb carbon: A review of graphene. *Chem. Rev.* **2010**, *110*, 132–145. [CrossRef] [PubMed]
104. Viculis, L.M.; Mack, J.J.; Kaner, R.B. A chemical route to carbon nanoscrolls. *Science* **2003**, *299*. [CrossRef] [PubMed]
105. Park, S.; Ruoff, R.S. Chemical methods for the production of graphenes. *Nat. Nanotechnol.* **2009**, *4*, 217–224. [CrossRef] [PubMed]
106. Jiao, L.Y.; Wang, X.R.; Diankov, G.; Wang, H.L.; Dai, H.J. Facile synthesis of high-quality graphene nanoribbons. *Nat. Nanotechnol.* **2010**, *5*, 321–325. [CrossRef] [PubMed]
107. Kosynkin, D.V.; Higginbotham, A.L.; Sinitskii, A.; Lomeda, J.R.; Dimiev, A.; Price, B.K.; Tour, J.M. Longitudinal unzipping of carbon nanotubes to form graphene nanoribbons. *Nature* **2009**, *458*, 872–876. [CrossRef] [PubMed]
108. Jiao, L.Y.; Zhang, L.; Wang, X.R.; Diankov, G.; Dai, H.J. Narrow graphene nanoribbons from carbon nanotubes. *Nature* **2009**, *458*, 877–880. [CrossRef] [PubMed]
109. Lin, T.; Liu, Z.; Zhou, M.; Bi, H.; Zhang, K.; Huang, F.; Wan, D.; Zhong, Y. Rapid microwave synthesis of graphene directly on h-BN with excellent heat dissipation performance. *ACS Appl. Mater. Interfaces* **2014**, *6*, 3088–3092. [CrossRef] [PubMed]
110. Xin, G.Q.; Hwang, W.; Kim, N.; Cho, S.M.; Chae, H. A graphene sheet exfoliated with microwave irradiation and interlinked by carbon nanotubes for high-performance transparent flexible electrodes. *Nanotechnology* **2010**, *21*. [CrossRef] [PubMed]
111. Shen, Y.; Jing, T.; Ren, W.; Zhang, J.; Jiang, Z.-G.; Yu, Z.-Z.; Dasari, A. Chemical and thermal reduction of graphene oxide and its electrically conductive polylactic acid nanocomposites. *Compos. Sci. Technol.* **2012**, *72*, 1430–1435. [CrossRef]
112. Cote, L.J.; Kim, F.; Huang, J. Langmuir-Blodgett assembly of graphite oxide single layers. *J. Am. Chem. Soc.* **2009**, *131*, 1043–1049. [CrossRef] [PubMed]
113. Loh, K.P.; Bao, Q.L.; Ang, P.K.; Yang, J.X. The chemistry of graphene. *J. Mater. Chem.* **2010**, *20*, 2277–2289. [CrossRef]
114. Moon, I.K.; Lee, J. Highly qualified reduced graphene oxides: The best chemical reduction. *Chem. Commun.* **2011**, *47*, 9681–9683. [CrossRef] [PubMed]

115. Chua, C.K.; Pumera, M. Chemical reduction of graphene oxide: A synthetic chemistry viewpoint. *Chem. Soc. Rev.* **2014**, *43*, 291–312. [CrossRef] [PubMed]
116. Chen, L.; Hernandez, Y.; Feng, X.; Mullen, K. From nanographene and graphene nanoribbons to graphene sheets: Chemical synthesis. *Angew. Chem. Int. Ed. Engl.* **2012**, *51*, 7640–7654. [CrossRef] [PubMed]
117. Barg, S.; Perez, F.M.; Ni, N.; Pereira, P.V.; Maher, R.C.; Garcia-Tunon, E.; Eslava, S.; Agnoli, S.; Mattevi, C.; Saiz, E. Mesoscale assembly of chemically modified graphene into complex cellular networks. *Nat. Commun.* **2014**, *5*, 4328. [CrossRef] [PubMed]
118. Ruoff, R. Graphene: Calling all chemists. *Nat. Nano* **2008**, *3*, 10–11. [CrossRef] [PubMed]
119. Paredes, J.I.; Villar-Rodil, S.; Martinez-Alonso, A.; Tascon, J.M.D. Graphene oxide dispersions in organic solvents. *Langmuir* **2008**, *24*, 10560–10564. [CrossRef] [PubMed]
120. Bianco, A.; Cheng, H.-M.; Enoki, T.; Gogotsi, Y.; Hurt, R.H.; Koratkar, N.; Kyotani, T.; Monthioux, M.; Park, C.R.; Tascon, J.M.D.; et al. All in the graphene family—A recommended nomenclature for two dimensional carbon materials. *Carbon* **2013**, *65*, 1–6. [CrossRef]
121. Poh, H.L.; Sanek, F.; Ambrosi, A.; Zhao, G.; Sofer, Z.; Pumera, M. Graphenes prepared by Staudenmaier, Hofmann and Hummer's methods with consequent thermal exfoliation exhibit very different electrochemical properties. *Nanoscale* **2012**, *4*, 3515–3522. [CrossRef] [PubMed]
122. Compton, O.C.; Nguyen, S.T. Graphene oxide, highly reduced graphene oxide, and graphene: Versatile building blocks for carbon-based materials. *Small* **2010**, *6*, 711–723. [CrossRef] [PubMed]
123. Dreyer, D.R.; Park, S.; Bielawski, C.W.; Ruoff, R.S. The chemistry of graphene oxide. *Chem. Soc. Rev.* **2010**, *39*, 228–240. [CrossRef] [PubMed]
124. Brodie, B.C. On the atomic weight of graphite. *Philos. Trans. R. Soc. Lond.* **1859**, *149*, 249–259. [CrossRef]
125. Staudenmaier, L. Verfahren zur darstellung der graphitsaure. *Ber. Dtsch. Chem. Ges.* **1898**, *31*, 1481–1487. [CrossRef]
126. Hummers, W.S., Jr.; Offeman, R.E. Preparation of graphitic oxide. *J. Am. Chem. Soc.* **1958**, *80*, 1339. [CrossRef]
127. Schniepp, H.C.; Li, J.L.; McAllister, M.J.; Sai, H.; Herrera-Alonso, M.; Adamson, D.H.; Prud'homme, R.K.; Car, R.; Saville, D.A.; Aksay, I.A. Functionalized single graphene sheets derived from splitting graphite oxide. *J. Phys. Chem. B* **2006**, *110*, 8535–8539. [CrossRef] [PubMed]
128. Gao, X.F.; Jang, J.; Nagase, S. Hydrazine and thermal reduction of graphene oxide: Reaction mechanisms, product structures, and reaction design. *J. Phys. Chem. C* **2010**, *114*, 832–842. [CrossRef]
129. Ramesha, G.K.; Sampath, S. Electrochemical reduction of oriented graphene oxide films: An in situ Raman spectroelectrochemical study. *J. Phys. Chem. C* **2009**, *113*, 7985–7989. [CrossRef]
130. Abdelsayed, V.; Moussa, S.; Hassan, H.M.; Aluri, H.S.; Collinson, M.M.; El-Shall, M.S. Photothermal deoxygenation of graphite oxide with laser excitation in solution and graphene-aided increase in water temperature. *J. Phys. Chem. Lett.* **2010**, *1*, 2804–2809. [CrossRef]
131. Ng, Y.H.; Lightcap, I.V.; Goodwin, K.; Matsumura, M.; Kamat, P.V. To what extent do graphene scaffolds improve the photovoltaic and photocatalytic response of TiO_2 nanostructured films? *J. Phys. Chem. Lett.* **2010**, *1*, 2222–2227. [CrossRef]
132. Golsheikh, A.M.; Lim, H.N.; Zakaria, R.; Huang, N.M. Sonochemical synthesis of reduced graphene oxide uniformly decorated with hierarchical ZnS nanospheres and its enhanced photocatalytic activities. *RSC Adv.* **2015**, *5*, 12726–12735. [CrossRef]
133. Vinodgopal, K.; Neppolian, B.; Lightcap, I.V.; Grieser, F.; Ashokkumar, M.; Kamat, P.V. Sonolytic design of graphene-Au nanocomposites. Simultaneous and sequential reduction of graphene oxide and Au(III). *J. Phys. Chem. Lett.* **2010**, *1*, 1987–1993. [CrossRef]
134. Voiry, D.; Yang, J.; Kupferberg, J.; Fullon, R.; Lee, C.; Jeong, H.Y.; Shin, H.S.; Chhowalla, M. High-quality graphene via microwave reduction of solution-exfoliated graphene oxide. *Science* **2016**, *353*, 1413–1416. [CrossRef] [PubMed]
135. Mills, A.; Le Hunte, S. An overview of semiconductor photocatalysis. *J. Photochem. Photobiol. A* **1997**, *108*, 1–35. [CrossRef]
136. Mahlambi, M.M.; Ngila, C.J.; Mamba, B.B. Recent developments in environmental photocatalytic degradation of organic pollutants: The case of Titanium dioxide nanoparticles—A review. *J. Nanomater.* **2015**, *2015*. [CrossRef]
137. Nosaka, Y.; Nosaka, A. Understanding hydroxyl radical ($^{\bullet}OH$) generation processes in photocatalysis. *ACS Energy Lett.* **2016**, *1*, 356–359. [CrossRef]

138. Zhang, Y.; Tan, Y.; Stormer, H.L.; Kim, P. Experimental observation of the quantum Hall effect and Berry's phase in graphene. *Nature* **2005**, *438*, 201–204. [CrossRef] [PubMed]
139. Teh, C.M.; Mohamed, A.R. Roles of titanium dioxide and ion-doped titanium dioxide on photocatalytic degradation of organic pollutants (phenolic compounds and dyes) in aqueous solutions: A review. *J. Alloys Compd.* **2011**, *509*, 1648–1660. [CrossRef]
140. Hager, S.; Bauer, R. Heterogeneous photocatalytic oxidation of organics for air purification by near UV irradiated titanium dioxide. *Chemosphere* **1999**, *38*, 1549–1559. [CrossRef]
141. Faraldos, M.; Bahamonde, A. Environmental applications of titania-graphene photocatalysts. *Catal. Today* **2017**, *285*, 13–28. [CrossRef]
142. Upadhyay, R.K.; Soin, N.; Ro, S.S. Role of graphene/metal oxide composites as photocatalysts, adsorbents and disinfectants in water treatment: A review. *RSC Adv.* **2014**, *4*, 3823–3851. [CrossRef]
143. Fujishima, A.; Rao, T.N.; Tryk, D.A. Titanium dioxide photocatalysis. *J. Photochem. Photobiol. C Photochem. Rev.* **2000**, *1*, 1–21. [CrossRef]
144. Hu, G.; Tang, B. Photocatalytic mechanism of graphene/titanate nanotubes photocatalyst under visible-light irradiation. *Mater. Chem. Phys.* **2013**, *138*, 608–614. [CrossRef]
145. Cruz, M.; Gomez, C.; Duran-Valle, C.J.; Pastrana-Martínez, L.M.; Faria, J.L.; Silva, A.M.T.; Faraldosa, M.; Bahamondea, A. Bare TiO_2 and graphene oxide TiO_2 photocatalysts on the degradation of selected pesticides and influence of the water matrix. *Appl. Surf. Sci.* **2017**, *416*, 1013–1021. [CrossRef]
146. Wang, C.; Cao, M.; Wang, P.; Ao, Y.; Hou, J.; Qian, J. Preparation of graphene-TiO_2 composites with enhanced photocatalytic activity for the removal of dye and Cr (VI). *Appl. Catal. A Gen.* **2014**, *473*, 83–89. [CrossRef]
147. Pastrana-Martínez, L.M.; Morales-Torres, S.; Likodimos, V.; José, L.; Figueiredo, J.L.; Faria, J.L.; Falaras, P.; Silva, A.M.T. Advanced nanostructured photocatalysts based on reduced graphene oxide-TiO_2 composites for degradation of diphenhydramine pharmaceutical and methyl orange dye. *Appl. Catal. B* **2012**, *123*, 241–256. [CrossRef]
148. Liu, S.; Sun, H.; Liu, S.; Wang, S. Graphene facilitated visible light photodegradation of methylene blue over titanium dioxide photocatalysts. *Chem. Eng. J.* **2013**, *214*, 298–303. [CrossRef]
149. Zhang, L.-W.; Fu, H.-B.; Zhu, Y.-F. Efficient TiO_2 photocatalysts from surface hybridization of TiO_2 particles with graphite-like carbon. *Adv. Funct. Mater.* **2008**, *18*, 2180–2189. [CrossRef]
150. Ren, L.; Qi, X.; Liu, Y.; Huang, Z.; Wei, X.; Li, J.; Yang, L.; Zhong, J. Upconversion-P25–graphene composite as an advanced sunlight driven photocatalytic hybrid material. *J. Mater. Chem.* **2012**, *22*, 11765–11771. [CrossRef]
151. Long, R.; English, N.J.; Prezhdo, O.V. Photo-induced charge separation across the graphene-TiO_2 interface is faster than energy losses: A time-domain ab initio analysis. *J. Am. Chem. Soc.* **2012**, *134*, 14238–14248. [CrossRef] [PubMed]
152. Rehman, S.; Ullah, R.; Butt, A.M.; Gohar, N.D. Strategies of making TiO_2 and ZnO visible light active. *J. Hazard. Mater.* **2009**, *170*, 560–569. [CrossRef] [PubMed]
153. Wu, H.; Wu, X.-L.; Wang, Z.-M.; Aoki, H.; Kutsuna, S.; Keiko Jimura, K.; Hayashi, S. Anchoring titanium dioxide on carbon spheres for high-performancevisible light photocatalysis. *Appl. Catal. B Environ.* **2017**, *207*, 255–266. [CrossRef]
154. Warkhade, S.K.; Gaikwad, G.S.; Zodape, S.P.; Pratap, U.; Maldhure, A.V.; Wankhade, A.V. Low temperature synthesis of pure anatase carbon doped titanium dioxide: An efficient visible light active photocatalyst. *Mater. Sci. Semicond. Process.* **2017**, *63*, 18–24. [CrossRef]
155. Jiang, W.J.; Zhu, Y.F.; Zhu, G.X.; Zhang, Z.J.; Chen, X.J.; Yao, W.Q. Three-dimensional photocatalysts with a network structure. *J. Mater. Chem. A* **2017**, *5*, 5661–5679. [CrossRef]
156. Williams, G.; Seger, B.; Kamat, P.V. TiO_2–graphene nanocomposites. UV-assisted photocatalytic reduction of graphene oxide. *ACS Nano* **2008**, *2*, 1487–1491. [CrossRef] [PubMed]
157. Pan, X.; Yang, M.-Q.; Tang, Z.R.; Xu, Y.-J. Noncovalently functionalized graphene-directed synthesis of ultralarge graphene-based TiO_2 nanosheet composites: Tunable morphology and photocatalytic applications. *J. Phys. Chem. C* **2014**, *118*, 27325–27335. [CrossRef]
158. Kamegawa, T.; Yamahana, D.; Yamashita, H. Graphene coating of TiO_2 nanoparticles loaded on mesoporous silica for enhancement of photocatalytic activity. *J. Phys. Chem. C* **2010**, *114*, 15049–15053. [CrossRef]

159. Bekyarova, E.; Itkis, M.E.; Ramesh, P.; Berger, C.; Sprinkle, M.; de Heer, W.A.; Haddon, R.C. Chemical modification of epitaxial graphene: Spontaneous grafting of aryl groups. *J. Am. Chem. Soc.* **2009**, *131*, 1336–1337. [CrossRef] [PubMed]
160. Zhang, Q.; Bao, N.; Wang, X.; Hu, X.; Miao, X.; Chaker, M.; Ma, D. Advanced fabrication of chemically bonded graphene/TiO_2 continuous fibers with enhanced broadband photocatalytic properties and involved mechanisms exploration. *Sci. Rep.* **2016**, *6*. [CrossRef] [PubMed]
161. Yao, Y.; Jie, G.; Bao, F.; Jiang, S.; Zhang, X.; Ma, R. Covalent functionalization of graphene with polythiophene through a Suzuki coupling reaction. *RSC Adv.* **2015**, *5*, 42754–42761. [CrossRef]
162. He, F.; Fan, J.; Ma, D.; Zhang, L.; Leung, C.; Chan, H.L. The attachment of Fe_3O_4 nanoparticles to graphene oxide by covalent bonding. *Carbon* **2010**, *48*, 3139–3144. [CrossRef]
163. Morawskia, A.W.; Kusiak-Nejmana, E.; Wanaga, A.; Kapica-Kozara, J.; Wróbela, R.J.; Ohtanib, B.; Aksienionekc, M.; Lipinska, L. Photocatalytic degradation of acetic acid in the presence of visiblelight-active TiO_2-reduced graphene oxide photocatalysts. *Catal. Today* **2017**, *280*, 108–113. [CrossRef]
164. Liu, Y.; Zhang, D.; Shang, Y.; Zang, W.; Li, M. Construction of multifunctional films based on graphene-TiO_2 composite materials for strain sensing and photodegradation. *RSC Adv.* **2015**, *5*, 104785–104791. [CrossRef]
165. Raliya, R.; Avery, C.; Chakrabarti, S.; Biswas, P. Photocatalytic degradation of methyl orange dye by pristine titanium dioxide, zinc oxide, and graphene oxide nanostructures and their composites under visible light irradiation. *Appl. Nanosci.* **2017**, *7*, 253–259. [CrossRef]
166. Kuila, T.; Bose, S.; Mishra, A.K.; Kharna, P.; Kim, N.H.; Lee, J.H. Recent advances in graphene based polymer composites. *Progress Mater. Sci.* **2012**, *57*, 1061–1105. [CrossRef]
167. Huang, X.; Qi, X.; Freddy Boeyab, F.; Zhang, H. Graphene-based composites. *Chem. Soc. Rev.* **2011**, *41*, 666–686. [CrossRef] [PubMed]
168. Bai, H.; Li, C.; Shi, G. Functional composite materials based on chemically converted graphene. *Adv. Mater.* **2011**, *23*, 1089–1115. [CrossRef] [PubMed]
169. Sreeprasad, T.S.; Berry, V. How do the electrical properties of graphene change with its functionalization? *Small* **2013**, *9*, 341–350. [CrossRef] [PubMed]
170. Pan, X.; Zhao, Y.; Liu, S.; Korzeniewski, C.L.; Wang, S.; Fan, Z. Comparing graphene-TiO_2 nanowire and graphene-TiO_2 nanoparticle composite photocatalysts. *ACS Appl. Mater. Interfaces* **2012**, *4*, 3944–3950. [CrossRef] [PubMed]
171. Lee, J.S.; You, K.H.; Park, C.B. Highly photoactive, low bandgap TiO_2 nanoparticles wrapped by graphene. *Adv. Mater.* **2012**, *24*, 1084–1088. [CrossRef] [PubMed]
172. Wang, J.; Salihi, E.C.; Šiller, L. Green reduction of graphene oxide using alanine. *Mater. Sci. Eng. C* **2017**, *72*, 1–6. [CrossRef] [PubMed]
173. Pei, S.; Cheng, H.-M. The reduction of graphene oxide. *Carbon* **2012**, *50*, 3210–3228. [CrossRef]
174. Bell, N.J.; Ng, Y.H.; Du, A.; Coster, H.; Smith, S.C.; Amal, R. Understanding the enhancement in photoelectrochemical properties of photocatalytically prepared TiO_2- reduced graphene oxide composite. *J. Phys. Chem. C* **2011**, *115*, 6004–6009. [CrossRef]
175. Zhang, Y.; Pan, C. TiO_2/graphene composite from thermal reaction of graphene oxide and its photocatalytic activity in visible light. *J. Mater. Sci.* **2011**, *46*, 2622–2626. [CrossRef]
176. Zhang, X.-Y.; Li, H.-P.; Cui, X.-L.; Linb, Y. Graphene/TiO_2 nanocomposites: Synthesis, characterization and application in hydrogen evolution from water photocatalytic splitting. *J. Mater. Chem.* **2010**, *20*, 2801–2806. [CrossRef]
177. Zabihi, F.; Ahmadian-Yazdi, M.-R.; Eslamian, M. Photocatalytic graphene-TiO_2 thin films fabricated by low-temperature ultrasonic vibration-assisted spin and spray coating in a sol-gel process. *Catalysts* **2017**, *7*, 136. [CrossRef]
178. Gopalakrishnan, A.; Binitha, N.N.; Yaakob, Z. Excellent photocatalytic activity of titania-graphene nanocomposites prepared by a facile route. *J. Sol-Gel Sci. Technol.* **2016**, *80*, 189–200. [CrossRef]
179. Shao, L.; Quan, S.; Liu, Y.; Guo, Z.; Wang, Z. A novel "gel-sol" strategy to synthesize TiO_2 nanorod combining reduced graphene oxide composites. *Mater. Lett.* **2013**, *107*, 307–310. [CrossRef]
180. Long, M.; Qin, Y.; Chen, C.; Guo, X.; Tan, B.; Cai, W. Origin of visible light photoactivity of reduced graphene oxide/TiO_2 by in situ hydrothermal growth of undergrown TiO_2 with graphene oxide. *J. Phys. Chem. C* **2013**, *117*, 16734–16741. [CrossRef]

181. Zhang, H.; Lv, X.; Li, Y.; Wang, Y.; Li, J. P25-graphene composite as a high performance photocatalyst. *ACS Nano* **2010**, *4*, 380–386. [CrossRef] [PubMed]
182. Hu, G.; Yang, J.; Zhao, D.; Chen, Y.; Cao, Y. Research on photocatalytic properties of TiO_2-graphene composites with different morphologies. *J. Mater. Eng. Perform.* **2017**, *26*, 3263–3270. [CrossRef]
183. Hamandi, M.; Berhault, G.; Guillard, C.; Kochkar, H. Reduced graphene oxide/TiO_2 nanotube composites for formic acid photodegradation. *Appl. Catal. B Environ.* **2017**, *209*, 203–213. [CrossRef]
184. Lv, S.; Wan, J.; Shen, Y.; Hu, Z. Preparation of superlong TiO_2 nanotubes and reduced graphene oxide composite photocatalysts with enhanced photocatalytic performance under visible light irradiation. *J. Mater. Sci. Mater. Electron.* **2017**, *28*, 14769–14776. [CrossRef]
185. Kusiak-Nejmana, E.; Wanaga, A.; Kowalczyka, L.; Kapica-Kozara, J.; Colbeau-Justinb, C.; Mendez Medrano, M.G.; Morawsk, A.W. Graphene oxide-TiO_2 and reduced graphene oxide-TiO_2 nanocomposites: Insight in charge-carrier lifetime measurements. *Catal. Today* **2017**, *287*, 189–195. [CrossRef]
186. Li, T.; Wang, T.; Qu, G.; Qu, G.; Liang, D.; Hu, S. Synthesis and photocatalytic performance of reduced graphene oxide-TiO_2 nanocomposites for orange II degradation under UV light irradiation. *Environ. Sci. Pollut. Res.* **2017**, *24*, 12416–12425. [CrossRef] [PubMed]
187. Yadav, H.M.; Kim, J.-S. Solvothermal synthesis of anatase TiO_2-graphene oxide nanocomposites and their photocatalytic performance. *J. Alloys Compd.* **2016**, *688*, 123–129. [CrossRef]
188. Hu, J.J.; Lia, H.; Muhammada, S.; Wua, Q.; Zhaoa, Y.; Jiaoa, Q. Surfactant-assisted hydrothermal synthesis of TiO_2/reduced graphene oxide nanocomposites and their photocatalytic performances. *J. Solid State Chem.* **2017**, *253*, 113–120. [CrossRef]
189. Ge, M.-Z.; Li, S.-H.; Huang, J.-Y.; Zhang, K.-Q.; Al-Deyabc, S.S.; Lai, Y.-K. TiO_2 nanotube arrays loaded with reduced graphene oxide films: Facile hybridization and promising photocatalytic application. *J. Mater. Chem. A* **2015**, *3*, 3491–3499. [CrossRef]
190. De Oliveira, A.G.; Nascimento, J.P.; de Fátima Gorgulho, H.; Martelli, P.B.; Furtado, C.A.; Figueiredo, J.L. Electrochemical synthesis of TiO_2/Graphene oxide composite films for photocatalytic applications. *J. Alloys Compd.* **2016**, *654*, 514–522. [CrossRef]
191. Shanmugam, M.; Alsalme, A.; Alghamdi, A.; Jayavel, R. In-situ microwave synthesis of graphene-TiO_2 nanocomposites with enhanced photocatalytic properties for the degradation of organic pollutants. *J. Photochem. Photobiol. B Biol.* **2016**, *163*, 216–223. [CrossRef] [PubMed]
192. Wang, H.; Gao, H.; Chen, M.; Xu, X.; Wang, X.; Pan, C.; Gao, J. Microwave-assisted synthesis of reduced graphene oxide/titania nanocomposites as an adsorbent for methylene blue adsorption. *J. Appl. Surf. Sci.* **2016**, *360*, 840–848. [CrossRef]
193. Yang, Y.; Liu, E.; Fan, J.; Hu, X.; Hou, W.; Wu, F.; Ma, Y. Green and facile microwave-assisted synthesis of TiO_2/graphene nanocomposite and their photocatalytic activity for methylene blue degradation. *Russ. J. Phys. Chem. A* **2014**, *88*, 478–483. [CrossRef]
194. Pu, S.; Zhu, R.; Ma, H.; Deng, D.; Pei, X.; Qi, F.; Chu, W. Facile in-situ design strategy to disperse TiO_2 nanoparticles on graphene for the enhanced photocatalytic degradation of rhodamine 6G. *Appl. Catal. B Environ.* **2017**, *218*, 208–219. [CrossRef]
195. Pokhrel, D.; Viraraghavan, T. Treatment of pulp and paper mill wastewater—A review. *Sci. Total Environ.* **2004**, *333*, 37–58. [CrossRef] [PubMed]
196. Liu, L.; Zhang, B.; Zhang, Y.; He, Y.; Huang, L.; Tan, S.; Cai, X. Simultaneous removal of cationic and anionic dyes from environmental water using montmorillonite-pillared graphene oxide. *J. Chem. Eng. Data* **2015**, *60*, 1270–1278. [CrossRef]
197. Bhullar, N.; Sharma, S.; Sud, D. Studies of adsorption for dye effluent and decolonization of methylene blue and methyl blue based on the surface of biomass adsorbent. *Pollut. Res.* **2012**, *31*, 681–686.
198. Hameed, B.H.; Din, A.T.M.; Ahmad, A.L. Adsorption of methylene blue onto bamboo-based activated carbon: Kinetics and equilibrium studies. *J. Hazard. Mater.* **2007**, *141*, 819–825. [CrossRef] [PubMed]
199. Mohamed, H.H. Biphasic TiO microspheres/reduced graphene oxide for effective simultaneous photocatalytic reduction and oxidation processes. *Appl. Catal. A Gen.* **2017**, *541*, 25–34. [CrossRef]
200. Zhang, N.; Li, B.; Li, S.; Yang, S. Graphene-supported mesoporous Titania nanosheets for efficient photodegradation. *J. Colloid Interface Sci.* **2017**, *505*, 711–718. [CrossRef] [PubMed]

201. Najafi, M.; Kermanpur, A.; Rahimipour, M.R.; Najafizadeh, A. Effect of TiO_2 morphology on structure of TiO_2-graphene oxide nanocomposite synthesized via a one-step hydrothermal method. *J. Alloys Compd.* **2017**, *722*, 272–277. [CrossRef]
202. Divya, K.S.; Madhu, A.K.; Umadevi, T.U.; Suprabha, T.; Radhakrishnan Nair, P.; Suresh, M. Improving the photocatalytic performance of TiO_2 via hybridizing with graphene. *J. Semiconduct.* **2017**, *38*. [CrossRef]
203. Sohail, M.; Xue, H.; Jiao, Q.; Li, H.; Khan, K.; Wang, S. Synthesis of well-dispersed TiO_2@reduced graphene oxide (rGO) nanocomposites and their photocatalytic properties. *Mater. Res. Bull.* **2017**, *90*, 125–130. [CrossRef]
204. Tseng, I.-H.; Sung, Y.-M.; Chang, P.-Y.; Lin, S.-W. Photocatalytic performance of Titania nanosheets templated by graphene oxide. *J. Photochem. Photobiol. A Chem.* **2017**, *339*, 1–11. [CrossRef]
205. Minella, M.; Sordello, F.; Minero, C. Photocatalytic process in TiO_2/graphene hybrid materials. Evidence of charge separation by electron transfer from reduced graphene oxide to TiO_2. *Catal. Today* **2017**, *281*, 29–37. [CrossRef]
206. Raja, V.; Shiamala, L. Biphasic TiO_2 nanoparticles decorated graphene nanosheets for visible light driven photocatalytic degradation of organic dyes. *Appl. Surf. Sci.* **2017**, *31*. [CrossRef]
207. Verma, R.; Samdarshi, S.K.; Sagar, K. Nanostructured bi-phasic TiO_2 nanoparticles grown on reduced graphene oxide with high visible light photocatalytic detoxification. *Mater. Chem. Phys.* **2017**, *186*, 202–211. [CrossRef]
208. Atchudan, R.; Jebakumar Immanuel Edison, T.N.; Perumal, S.; Karthikeyan, D.; Lee, Y.R. Effective photocatalytic degradation of anthropogenic dyes using graphene oxide grafting titanium dioxide nanoparticles under UV-light irradiation. *J. Photochem. Photobiol. A Chem.* **2017**, *333*, 92–104. [CrossRef]
209. Darvishi, M.; Seyed-Yazdi, J. Characterization and comparison of photocatalytic activities of prepared TiO_2/graphene nanocomposites using titanium butoxide and TiO_2 via microwave irradiation method. *Mater. Res. Express* **2016**, *3*. [CrossRef]
210. Rezaei, M.; Salem, S. Photocatalytic activity enhancement of anatase-graphene nanocomposite for methylene removal: Degradation and kinetics. *Spectrochim. Acta A Mol. Biomol. Spectrosc.* **2016**, *167*, 41–49. [CrossRef] [PubMed]
211. Rezaei, M.; Salem, S. Optimal TiO_2-graphene oxide nanocomposite for photocatalytic activity under sunlight condition: Synthesis, characterization, and kinetics. *Int. J. Chem. Kinet.* **2016**, *48*, 573–583. [CrossRef]
212. Charoensuk, J.; Charupongtawitch, R.; Usakulwattana, A. Kinetics of photocatalytic degradation of methylene blue by TiO_2-graphene nanocomposites. *J. Nanosci. Nanotechnol.* **2016**, *16*, 296–302.
213. Wang, R.; Yang, R.; Wang, B. Efficient degradation of methylene blue by the nano TiO_2-functionalized graphene oxide nanocomposite photocatalyst for wastewater treatment. *Water Air Soil Pollut.* **2016**, *227*. [CrossRef]
214. Liu, G.; Wang, R.; Liu, H.; Han, K.; Cui, H. Highly dispersive nano-TiO_2 in situ growing on functional graphene with high photocatalytic activity. *J. Nanopart. Res.* **2016**, *18*, 1–8. [CrossRef]
215. Baldissarelli, V.Z.; De Souza, T.; Andrade, L.; Oliveira, L.F.C.D.; José, H.J. Preparation and photocatalytic activity of TiO_2-exfoliated graphite oxide composite using an ecofriendly graphite oxidation method. *Appl. Surf. Sci.* **2015**, *359*, 868–874. [CrossRef]
216. Gu, L.; Zhang, H.; Jiao, Z.; Li, M.; Wu, M.; Lei, Y. Glucosamine-induced growth of highly distributed TiO_2 nanoparticles on graphene nanosheets as high-performance photocatalysts. *RSC Adv.* **2016**, *6*, 67039–67048. [CrossRef]
217. Fan, J.; Liu, E.; Hu, X.; Ma, Y.; Fan, X.; Li, Y.; Tang, C. Facile hydrothermal synthesis of TiO_2 nanospindles-reduced graphene oxide composite with a enhanced photocatalytic activity. *J. Alloys Compd.* **2015**, *623*, 298–303.
218. Sun, M.; Li, W.; Sun, S.; He, J.; Zhang, Q.; Shi, Y. One-step in situ synthesis of graphene-TiO_2 nanorod hybrid composites with enhanced photocatalytic activity. *Mater. Res. Bull.* **2015**, *61*, 280–286. [CrossRef]
219. Rong, X.; Qiu, F.; Zhang, C.; Fu, L.; Wang, Y.; Yang, D. Preparation, characterization and photocatalytic application of TiO_2-graphene photocatalyst under visible light irradiation. *Ceram. Int.* **2015**, *41*, 2502–2511. [CrossRef]
220. Gupta, B.K.; Kedawat, G.; Agrawal, Y.; Kumar, P.; Dwivedi, J. A novel strategy to enhance ultraviolet light driven photocatalysis from graphene quantum dots infilled TiO_2 nanotube arrays. *RSC Adv.* **2015**, *5*, 10623–10631. [CrossRef]

221. Sha, J.; Zhao, N.; Liu, E.; Shi, C.; He, C.; Li, J. In situ synthesis of ultrathin 2-D TiO_2 with high energy facets on graphene oxide for enhancing photocatalytic activity. *Carbon* **2014**, *68*, 352–359. [CrossRef]
222. Yang, Y.; Xu, L.; Wang, H.; Wang, W.; Zhang, L. TiO_2/graphene porous composite and its photocatalytic degradation of methylene blue. *Mater. Des.* **2016**, *108*, 632–639. [CrossRef]
223. Suave, J.; Amorim, S.M.; Moreira, R.F.P.M. TiO_2-graphene nanocomposite supported on floating autoclaved cellular concrete for photocatalytic removal of organic compounds. *J. Environ. Chem. Eng.* **2017**, *5*, 3215–3223. [CrossRef]
224. Ai, L.; Zhang, C.; Meng, L. Adsorption of methyl orange from aqueous solution on hydrothermal synthesized Mg–Al layered double hydroxide. *J. Chem. Eng. Data* **2011**, *56*, 4217–4225. [CrossRef]
225. Lavanya, T.; Dutta, M.; Ramaprabhu, S.; Satheesh, K. Superior photocatalytic performance of graphene wrapped anatase/rutile mixed phase TiO_2 nanofibers synthesized by a simple and facile route. *J. Environ. Chem. Eng.* **2017**, *5*, 494–503. [CrossRef]
226. Hou, X.; Sun, T.; Zhao, X. Calcination of reduced graphene oxide decorated TiO_2 composites for recovery and reuse in photocatalytic applications. *Ceram. Int.* **2017**, *43*, 1150–1159.
227. Zhao, F.; Dong, B.; Gao, R.; Su, G.; Liu, W.; Shi, L.; Xia, C. A three-dimensional graphene-TiO_2 nanotube nanocomposite with exceptional photocatalytic activity for dye degradation. *Appl. Surf. Sci.* **2015**, *351*, 303–308. [CrossRef]
228. Lu, Z.; Chen, G.; Hao, W.; Sun, G.; Li, Z. Mechanism of UV-assisted TiO_2/reduced graphene oxide composites with variable photodegradation of methyl orange. *RSC Adv.* **2015**, *5*, 72916–72922. [CrossRef]
229. Xia, H.Y.; He, G.Q.; Min, Y.L.; Liu, T. Role of the crystallite phase of TiO_2 in graphene/TiO_2 photocatalysis. *J. Mater. Sci. Mater. Electron.* **2015**, *26*, 3357–3363. [CrossRef]
230. Jiang, Y.; Wang, W.-N.; Biswas, P.; Fortner, J.D. Facile aerosol synthesis and characterization of ternary crumpled graphene-TiO_2-magnetite nanocomposites for advanced watertreatment. *ACS Appl. Mater. Interfaces* **2014**, *6*, 11766–11774. [CrossRef] [PubMed]
231. Han, W.; Ren, L.; Zhang, Z.; Qi, X.; Liu, Y.; Huang, Z.; Zhong, J. Graphene-supported flocculent-like TiO_2 nanostructures for enhanced photoelectrochemical activity and photodegradation performance. *J. Ceram. Int.* **2015**, *41*, 7471–7477. [CrossRef]
232. Lavanya, T.; Satheesh, K.; Dutta, M.; Victor Jaya, N. Superior photocatalytic performance of reduced graphene oxide wrapped electrospun anatase mesoporous TiO_2 nanofibers. *J. Alloys Compd.* **2014**, *615*, 643–650. [CrossRef]
233. Wang, Y.; Li, Z.; He, Y.; Li, F.; Liu, X. Low-temperature solvothermal synthesis of graphene-TiO_2 nanocomposite and its photocatalytic activity for dye degradation. *Mater. Lett.* **2014**, *134*, 115–118. [CrossRef]
234. Athanasekou, C.P.; Morales-Torres, S.; Likodimos, V.; Romanos, G.E.; Pastrana-Martinez, L.M.; Falaras, P.; Faria, J.L.; Figueiredo, J.L. Prototype composite membranes of partially reduced graphene oxide/TiO_2 for photocatalytic ultrafiltration water treatment under visible light. *Appl. Catal. B Environ.* **2014**, *158–159*, 361–372. [CrossRef]
235. Liu, Y. Hydrothermal synthesis of TiO_2-RGO composites and their improved photocatalytic activity in visible light. *RSC Adv.* **2014**, *4*, 36040–36045. [CrossRef]
236. Shakir, K.; Elkafrawy, A.F.; Ghoneimy, H.F.; Elrab Beheir, S.G.; Refaat, M. Removal of rhodamine B (a basic dye) and thoron (an acidic dye) from dilute aqueous solutions and wastewater simulants by ion flotation. *Water Res.* **2010**, *44*, 1449–1461. [CrossRef] [PubMed]
237. Chen, Q.; Zhou, M.; Zhang, Z.; Tang, T.; Wang, T. Preparation of TiO_2 nanotubes/reduced graphene oxide binary nanocomposites enhanced photocatalytic properties. *J. Mater. Sci. Mater. Electron.* **2017**, *28*, 9416–9422. [CrossRef]
238. Chen, Y.; Dong, X.; Cao, Y.; Xiang, J. Enhanced photocatalytic activities of low-bandgap TiO_2-reduced graphene oxide nanocomposites. *J. Nanopart. Res.* **2017**, *19*. [CrossRef]
239. Wang, W.; Huang, X.; Lai, M. RGO/TiO_2 nanosheets immobilized on magnetically actuated artificial cilia film: A new mode for efficient photocatalytic reaction. *RSC Adv.* **2017**, *7*, 10517–10523. [CrossRef]
240. Biris, A.R.; Toloman, D.; Popa, A.; Lazar, M.D.; Kannarpady, G.K.; Saini, V.; Watanabe, F.; Chhetri, B.P.; Ghosh, A. Synthesis of tunable core-shell nanostructures based on TiO_2-graphene architectures and their application in the photodegradation of rhodamine dyes. *Phys. E Low Dimens. Syst. Nanostruct.* **2016**, *81*, 326–333. [CrossRef]

241. Kim, T.-W.; Park, M.; Kim, H.Y.; Park, S.-J. Preparation of flower-like TiO_2 sphere/reduced graphene oxide composites for photocatalytic degradation of organic pollutants. *J. Solid State Chem.* **2016**, *239*, 91–98. [CrossRef]
242. Liu, H.; Wang, Y.; Shi, L.; Xu, R.; Huang, L.; Tan, S. Utilization of reduced graphene oxide for the enhancement of photocatalytic property of TiO_2 nanotube. *Desalination Water Treat.* **2016**, *57*, 13263–13272. [CrossRef]
243. Sedghi, R.; Heidari, F. A novel & effective visible light-driven TiO_2/magnetic porous graphene oxide nanocomposite for the degradation of dye pollutants. *RSC Adv.* **2016**, *6*, 49459–49468.
244. Zhang, J.-J.; Wu, Y.-H.; Mei, J.-Y.; Zheng, G.-P.; Yan, T.-T.; Zheng, X.-C.; Liu, P.; Guan, X.-X. Synergetic adsorption and photocatalytic degradation of pollutants over 3D TiO_2-graphene aerogel composites synthesized: Via a facile one-pot route. *Photochem. Photobiol. Sci.* **2016**, *15*, 1012–1019. [CrossRef] [PubMed]
245. He, R.; He, W. Ultrasonic assisted synthesis of TiO_2-reduced graphene oxide nanocomposites with superior photovoltaic and photocatalytic activities. *Ceram. Int.* **2016**, *42*, 5766–5771. [CrossRef]
246. Fang, R.; Liang, Y.; Ge, X.; Du, M.; Li, S.; Li, T. Preparation and photocatalytic degradation activity of TiO_2/rGO/polymer composites. *Colloid Polym. Sci.* **2015**, *293*, 1151–1157. [CrossRef]
247. Liang, D.; Cui, C.; Hub, H.; Wang, Y.; Xu, S.; Ying, B.; Li, P.; Lu, B. One-step hydrothermal synthesis of anatase TiO_2/reduced graphene oxide nanocomposites with enhanced photocatalytic activity. *J. Alloys Compd.* **2014**, *582*, 236–240. [CrossRef]
248. Li, Q.; Bian, J.; Zhang, L.; Zhang, R.; Wang, G. Synthesis of carbon materials-TiO_2 hybrid nanostructures and their visible-light photo-catalytic activity. *Chem Plus Chem* **2014**, *79*, 454–461.
249. Rajoriya, S.; Bargole, S.; Saharan, V.K. Degradation of a cationic dye (Rhodamine 6G) using hydrodynamic cavitation coupled with other oxidative agents: Reaction mechanism and pathway. *Ultrason. Sonochem.* **2017**, *34*, 183–194. [CrossRef] [PubMed]
250. Dai, B.; Tao, H.; Lin, Y.-J.; Chang, C.-T. Study of various nanostructures Titania with graphene composites: The preparation and photocatalytic activities. *Nano* **2016**, *11*. [CrossRef]
251. Liang, X.; Tao, H.; Zhang, Q. High performance photocatalytic degradation by graphene/titanium nanotubes under near visible light with low energy irradiation. *J. Nanosci. Nanotechnol.* **2015**, *15*, 4887–4894. [CrossRef] [PubMed]
252. Zhang, Q.; Liang, X.; Chen, B.-Y.; Chang, C. Deciphering effects of functional groups and electron density on azodyes degradation by graphene loaded TiO_2. *Appl. Surf. Sci.* **2015**, *357*, 1064–1071. [CrossRef]
253. Posa, V.R.; Annavaram, V.; Somala, A.R. Fabrication of graphene-TiO_2 nanocomposite with improved photocatalytic degradation for acid orange 7 dye under solar light irradiation. *Bull. Mater. Sci.* **2016**, *39*, 759–767. [CrossRef]
254. Gao, P.; Li, A.; Sun, D.D.; Ng, W.J. Effects of various TiO_2 nanostructures and graphene oxide on photocatalytic activity of TiO_2. *J. Hazard. Mater.* **2014**, *279*, 96–104. [CrossRef] [PubMed]
255. Muthirulan, P.; Devi, C.N.; Sundaram, M.M. TiO_2 wrapped graphene as a high performance photocatalyst for acid orange 7 dye degradation under solar/UV light irradiations. *Ceram. Int.* **2014**, *40*, 5945–5957. [CrossRef]